Ultraviolet extrapolations in finite oscillator bases

S. König,[1,*] S. K. Bogner,[2,†] R. J. Furnstahl,[1,‡] S. N. More,[1,§] and T. Papenbrock[3,4,¶]

[1] *Department of Physics, The Ohio State University, Columbus, Ohio 43210, USA*
[2] *National Superconducting Cyclotron Laboratory and Department of Physics and Astronomy, Michigan State University, East Lansing, Michigan 48844, USA*
[3] *Department of Physics and Astronomy, University of Tennessee, Knoxville, Tennessee 37996, USA*
[4] *Physics Division, Oak Ridge National Laboratory, Oak Ridge, Tennessee 37831, USA*

(Dated: December 30, 2014)

The use of finite harmonic oscillator spaces in many-body calculations introduces both infrared (IR) and ultraviolet (UV) errors. The IR effects are well approximated by imposing a hard-wall boundary condition at a properly identified radius $L_{\rm eff}$. We show that duality of the oscillator implies that the UV effects are equally well described by imposing a sharp momentum cutoff at a momentum $\Lambda_{\rm eff}$ complementary to $L_{\rm eff}$. By considering two-body systems with separable potentials, we show that the UV energy corrections depend on details of the potential, in contrast to the IR energy corrections, which depend only on the S-matrix. An adaptation of the separable treatment to more general interactions is developed and applied to model potentials as well as to the deuteron with realistic potentials. The previous success with a simple phenomenological form for the UV error is also explained. Possibilities for controlled extrapolations for $A > 2$ based on scaling arguments are discussed.

arXiv:1409.5997v2 [nucl-th] 29 Dec 2014

I. INTRODUCTION

When truncated harmonic oscillator (HO) model spaces are used in wavefunction-based methods for computing atomic nuclei, both the infrared (IR) and the ultraviolet (UV) physics is modified, leading to systematic errors in observables [1–6]. If these errors can be understood formally, then controlled extrapolations to the results for the full model space can be made. A theoretical formulation for IR extrapolations was proposed in Ref. [5], and further developed in Refs. [7–9]. In this paper we provide a corresponding theoretical basis for UV extrapolations.

The IR effect of an oscillator basis truncation is practically the same as imposing a hard-wall boundary condition (*i.e.*, a sharp cutoff in position space) at a radius $L_{\rm eff}$. This is a low-momentum equivalence in the sense of an effective theory; we determine $L_{\rm eff}$ by matching the smallest eigenvalue of the squared momentum operator in the finite basis to the smallest eigenvalue in the spherical box. The quantity $L_{\rm eff}$ depends on the number of fermions [9]. For two-body bound states, expansions for the corrections to the energy and other observables based on a continuation of the S-matrix have been derived in Ref. [8] to next-to-leading order (NLO). At leading order (LO), the energy correction is proportional to $\exp\left(-2kL_{\rm eff}\right)$, with k given by the separation energy, due to the exponential fall-off of the wavefunction in position space. Further tests for oxygen isotopes show that the LO form of the corrections works very well for $A > 2$ (although the coefficients are fit rather than given as for $A = 2$) [9]. In those tests, it was possible (for coupled-cluster calculations with moderately soft potentials) to suppress the UV corrections by going to large values of the oscillator frequency Ω, so that the IR correction could be isolated.

However, the need to understand UV corrections remains. For many methods the full suppression of the UV is not feasible, and in all cases the UV effect is a systematic error that must be quantified. In addition, this error worsens for harder nucleon–nucleon potentials that may still be of interest. Finally, we seek an understanding of the successes (and limitations) of previous phenomenological forms. Thus we are well motivated to study the UV errors.

Here we follow the strategy of Refs. [7] and [8] by focusing on the two-body problem and exactly solvable examples to establish the true UV behavior for these simple systems. In doing so, the duality of the HO tells us that part of the IR lesson carries over; namely that the effect of the oscillator truncation in the UV is practically the same as a hard cutoff in momentum at an appropriate $\Lambda_{\rm eff}$, with an expression equivalent to $L_{\rm eff}$ when each is expressed in dimensionless units. This is demonstrated in Sec. II (and Appendix A).

However, the impact of this cutoff is not dual. While the IR result for the bound-state energy depends only on observables (and is therefore the same for any two interactions that predict the same S-matrix elements), the UV correction depends on the high-momentum behavior of the potential, which is not an observable. In Sec. III, we demonstrate this explicitly and derive a correction formula by considering a rank-one separable potential with a super-Gaussian form such as those used for effective field theory regulators. We then adapt the separable formulation to more general potentials by building on the classic work by Ernst *et al.* [10]. A fitting procedure for

* koenig.389@osu.edu
† bogner@nscl.msu.edu
‡ furnstahl.1@osu.edu
§ more.13@osu.edu
¶ tpapenbr@utk.edu

UV extrapolation is established, tested with model potentials, and, finally, applied to the deuteron calculated using realistic nucleon–nucleon interactions.

A phenomenological scheme for UV corrections based on a Gaussian ansatz, applicable to interactions evolved by the similarity renormalization group (SRG), was proposed in Ref. [5] without formal justification. It was also used for $A > 2$ with apparent success in Ref. [11]. Other works in the literature have also found that such an ansatz works well (although they have not generally treated the IR and UV parts separately). These successes might seem puzzling in light of our more general results, but we show in Sec. IV how the phenomenological ansatz arises when fitting in a narrow window in Λ_{eff}. Some further remarks on generalizing the separable-approximation approach are given in Sec. V, and in Sec. VI we summarize our results and provide an outlook on extensions of the UV extrapolations to $A > 2$.

II. BASIS TRUNCATION AND UV CUTOFF

In this section we discuss the relation between the basis size N and the frequency Ω of a finite oscillator model space and the corresponding UV cutoff Λ_{eff} in momentum space for a two-body system. Our notation and conventions are summarized in Appendix A, where we also give a detailed derivation of the results stated in the following.

A. Duality and momentum-space boxes

References [7] and [8] demonstrated that a truncated oscillator basis with highest excitation energy $N\Omega$ effectively imposes a spherical hard-wall boundary condition at a radius depending on N and b. The optimal effective radius L_{eff} can be determined by matching the smallest eigenvalue κ^2 of the squared momentum operator p^2 in the finite basis to the corresponding eigenvalue of the spherical box, namely $\kappa = \pi/L$ (for $\ell = 0$). The value can be established numerically, but an accurate approximation for the two-body system is [7]

$$L_{\text{eff}} = L_2 \equiv \sqrt{2(N + 3/2 + 2)}b\,. \tag{1}$$

Note that L_2 differs by $\mathcal{O}(1/N)$ from the naive estimate $L_0 \equiv \sqrt{2(N + 3/2)}b$. In localized bases that differ from the harmonic oscillator, L can also be determined from a numerical diagonalization of the operator p^2.

The dual nature of the harmonic oscillator Hamiltonian (A1) (*i.e.*, under $p \leftrightarrow \mu\Omega r$) implies that the truncation of the basis will effectively impose a sharp cutoff at a momentum Λ_{eff} depending only on N and b. The analog matching condition leads us to consider the smallest eigenvalue (denoted ρ) of the operator r^2 evaluated in that truncated basis. This eigenvalue is identical to the smallest (squared) distance that can be realized in the oscillator basis. Thus it corresponds to a lattice spacing on a grid and therefore sets the highest momentum available. As we see in Fig. 4, the square root of the largest eigenvalue of the squared momentum operator, which might be a natural guess for the effective UV cutoff, is not an accurate estimate for Λ_{eff}.

The smallest eigenvalue ρ is determined by Eqs. (A21) and (A27) in Appendix A. From steps completely analogous (dual) to those given in Refs. [7, 8] for the IR case, we find that the solution (in a subspace with fixed angular momentum ℓ) is

$$\rho = \frac{x_\ell b}{\sqrt{2}}\left(N + \frac{3}{2} + \Delta\right)^{-1/2} \tag{2}$$

with $\Delta = 2$ to leading order. The constant x_ℓ in the prefactor is the first positive zero of the spherical Bessel function j_ℓ. Since the UV cutoff is given by x_ℓ/ρ, it drops out again in our final result:

$$\Lambda_2 \equiv \sqrt{2(N + 3/2 + 2)}/b\,. \tag{3}$$

Hence, we have shown that the proper effective UV cutoff imposed by the basis truncation is given by Λ_2, which differs by a correction term from the naive estimate

$$\Lambda_0 \equiv \sqrt{2(N + 3/2)}/b \tag{4}$$

that one obtains by simply considering the maximum single-particle energy level represented by the truncated basis. We note that subleading corrections to $\Delta = 2$, which by duality apply equally to the IR and UV cutoff, are derived in Appendix A 4.

B. Isolating UV corrections

For an oscillator basis truncation with general b and N, both IR and UV errors will be significant. However, by choosing appropriate ranges of these parameters we can isolate one or the other and thereby analyze them separately (with the combined effect to be considered in future work). In Fig. 1(a) we plot the relative error in the deuteron energy $\Delta E_d/E_d$ for a large set of basis parameters with $4 < N < 100$ and $1\,\text{MeV} < \Omega < 100\,\text{MeV}$ against the value of L_2 (recall $\Omega = 1/\mu b^2$) from Eq. (1). The calculations use the 500 MeV N^{3}LO nucleon-nucleon NN potential of Entem and Machleidt [12], evolved by the SRG [13] to $\lambda = 2\,\text{fm}^{-1}$. For sufficiently large Ω, above a minimum N all points collapse to a single exponential curve that runs over six decades (at which point numerical errors in the calculation are reached and cause the curve to flatten)[1]). These are the UV-converged

[1] This effect is analogous to what is shown in Fig. 4 in Ref. [4]. Once the calculation is converged in the UV regime, the curves in such error plots flatten out at a value determined by whatever else limits the precision of the calculation. In Fig. 4 in Ref. [4], the value of the plateau is different for each curve because the data points have not been filtered to ensure convergence in the IR. In our case, the value is determined by the numerical precision of the calculation, which is reflected in the fact that the plateaus are the same in Figs. 1 and 2.

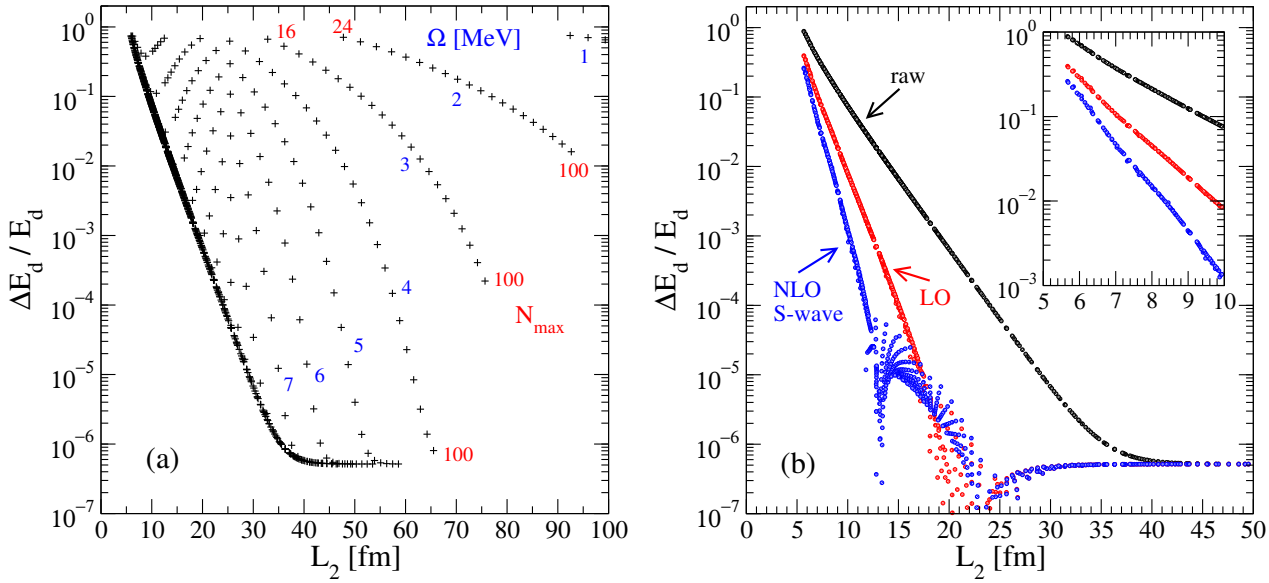

FIG. 1. (Color online) (a) Relative error in the deuteron energy, computed in harmonic-oscillator bases, for a wide range of oscillator parameters N and Ω as a function of $L_2(N,\Omega)$. Red labels mark the minimum and maximum N along sequences of constant Ω (indicated by blue labels along the sequence of crosses). These calculations use the N^{3}LO NN potential with a 500 MeV regulator cutoff from Ref. [12], which was evolved by the similarity renormalization group [13] to $\lambda = 2\,\mathrm{fm}^{-1}$. (b) Subset of calculations from (a) for which the UV correction can be neglected compared to the IR correction ("raw"), with LO and NLO corrections subtracted as described in the text. Inset: Curves for the lowest values of L_2.

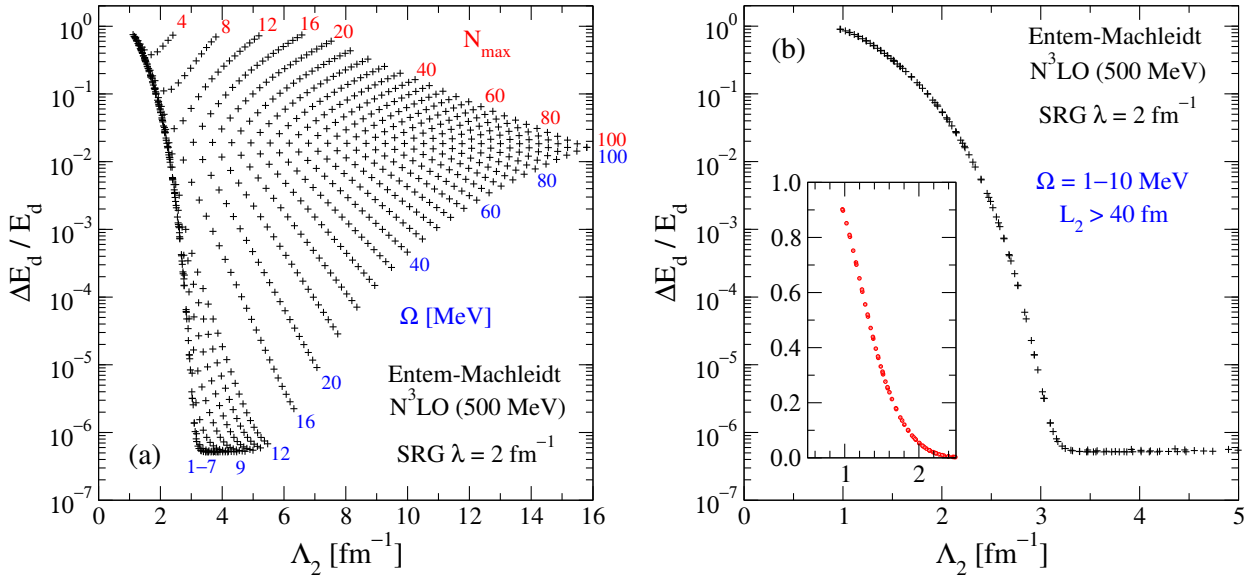

FIG. 2. (Color online) (a) Oscillator calculations of the relative error in the deuteron energy for a wide range of oscillator parameters N and Ω as a function of $\Lambda_2(N,\Omega)$. These are the same calculations as in Fig. 1. (b) Subset of calculations from (a) for which the IR correction can be neglected compared to the UV correction. Inset: linear plot.

points; that is, those for which the UV correction is much smaller than the IR correction.

In Fig. 1(b) these same UV-converged points are plotted (labeled "raw"). They are seen to form a smooth line with little spread; this is a signature that L_2 is the correct variable for the effective box size [7, 8] (if L_0 were used instead there would be a small but noticeable scatter). It is also evident from the straightness of the line on a semi-log plot that the functional form is dominantly an exponential over most of the range of $\Delta E_d/E_d$. This exponential is predicted by the systematic expansion derived in Refs. [5, 7, 8], for which successive orders are suppressed by powers of $e^{-2k_\infty L_2}$, where k_∞ is the deuteron binding momentum. (There are also pre-factors that are

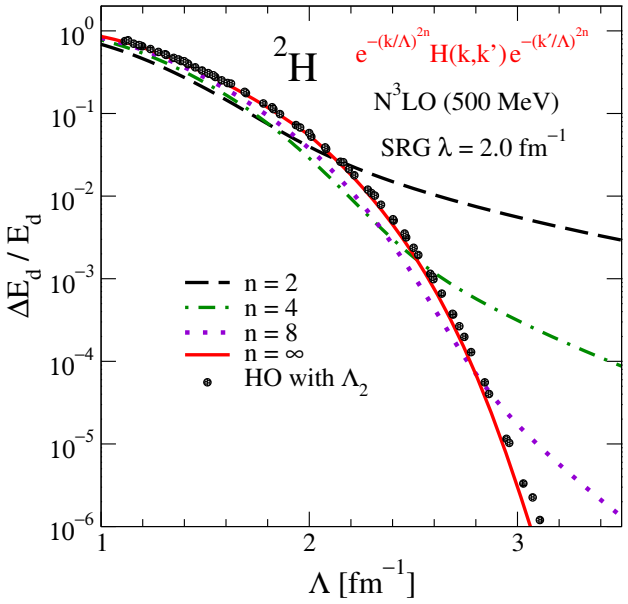

FIG. 3. (Color online) Calculations of the relative error in the deuteron energy as a function of $\Lambda_2(N,\Omega)$. Circles represent a wide range of oscillator parameters N and Ω that are IR converged. The series of lines shows energies for which the Hamiltonian has been smoothly cutoff with exponent n. The solid line corresponds to a sharp cutoff.

low-order polynomials in L_2.) If we subtract the leading correction, the result is the steeper exponential (proportional to $e^{-4k_\infty L_2}$) labeled "LO." Finally, if we subtract the NLO correction for only the S-wave part, we get the still steeper exponential ("NLO S-wave"), which is valid down to 10^{-5}. Thus we conclude that the IR corrections are well understood for the deuteron. What is not evident from these plots alone, but is documented in Ref. [7], is that the same results in Fig. 1(b) would be obtained with another potential as long as it was S-matrix equivalent at low energies (same phase shifts and deuteron properties, as from a unitary transformation). In this sense, the IR corrections are universal.

Next we try in Fig. 2(a) to isolate the IR-converged points with an analogous plot of the relative error in the deuteron energy but now as a function of Λ_2. There is a much greater spread of points, indicating that it is more difficult to have the IR error much smaller than the UV error, at least for a conventional range of Ω. However, for very low Ω we do find points collapsed to a single curve. These points, for which $L_2 > 40\,\mathrm{fm}$ (to reach IR errors smaller than UV errors), are plotted in Fig. 2(b). Just as in the case of isolated IR corrections, we find that a signature both of IR convergence and that Λ_2 is the appropriate variable is a smooth curve with little scatter of points. But the functional dependence is manifestly *not* dual: there are no straight-line segments in a semi-log plot. The phenomenological treatment of the UV correction suggested in Ref. [5] for SRG-evolved potentials used an ansatz for which $\Delta E_d/E_d \propto e^{-b_1\Lambda_2^2}$ (although Λ_0 instead of Λ_2 was actually used in [5], this difference is not significant for the present discussion). As we demonstrate in Sec. IV B, this form works for a limited range in Λ_2 but is not generally applicable.

To develop a theoretical understanding of UV corrections, we first validate the claim that the error from oscillator basis truncation is well reproduced by applying instead a sharp cutoff in momentum at Λ_2. In Fig. 3, the calculations from Fig. 2(b) are plotted as a function of $\Lambda = \Lambda_2(N,\Omega)$ along with several other functions of Λ given by the relative error from the same Hamiltonian, but now smoothly cut off as

$$H_{\mathrm{cut}}(k,k') = e^{-(k^2/\Lambda^2)^n} H(k,k') e^{-(k'^2/\Lambda^2)^n}, \qquad (5)$$

for $n = 2, 4, 8$ and ∞. The latter corresponds to a sharp cutoff. We find that the curve from a sharp cutoff tracks the truncated-oscillator points through many orders of magnitude. Finally, Fig. 4 shows the relative error when plotted against three cutoff variables, Λ_2, Λ_0, and $\Lambda_{\kappa_{\max}}$. The latter is defined as the square root of the largest eigenvalue of the squared momentum operator in the finite oscillator basis, which one might naively expect to be a natural choice. However, of the cases considered this actually gives the largest scatter in data. From the fact that we get an essentially smooth curve only for Λ_2, we conclude that this identification of the relevant UV cutoff is correct.

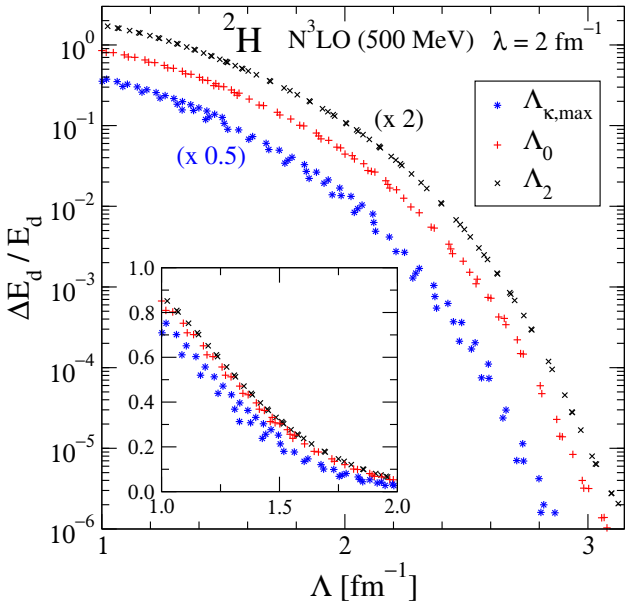

FIG. 4. (Color online) Relative error of deuteron binding energy plotted vs. lengths Λ_2, Λ_0, and $\Lambda_{\kappa,\max}$ (multiplied by factors 2, 1, and 1/2, respectively, to separate the curves. Inset: The same values on a linear scale and without the separation factors.

In the next section we take this correspondence as given and study a model Hamiltonian for which we can analyze the UV correction exactly.

III. SEPARABLE TWO-BODY INTERACTIONS

In this section we show that the UV error from oscillator basis truncations in the two-body problem can be determined exactly for any rank-one separable interaction by applying the effective sharp-momentum cutoff. We demonstrate that, unlike the case for IR corrections, the UV corrections depend on the high-momentum behavior of the potential. We derive an explicit correction formula for separable potentials and then adapt the approach to more general potentials, which leads to a practical fitting procedure.

A. Regularized contact interaction

Let us consider two particles interacting via an S-wave ($\ell = 0$) rank-one separable interaction of the form

$$V(\mathbf{k}, \mathbf{k}') = V(k', k) = a\, f_\lambda(k') f_\lambda(k)\,. \tag{6}$$

While most of the following derivation is actually more general, we will consider below the case of non-negative, dimensionless regulator functions $f_\lambda(k)$ that satisfy $f_\lambda(0) = 1$ and $f_\lambda \to 0$ for $k/\lambda \to \infty$. The potential (6) is then just a regularized contact interaction as it would arise, for example, from a low-energy effective field theory, and the coupling constant a is a length scale related (up to some rescaling factors) to an S-wave scattering length. For convenience, in this section we work in units with $2\mu = 1$, where μ is the reduced mass of the two-particle system. We focus on the single bound state (assuming that a is negative and large enough) with energy $E_\infty \equiv -\kappa_\infty^2$ and momentum-space wavefunction $\phi(k)$.[2] Thus κ_∞ is the binding momentum. The Schrödinger equation for $\phi(k)$ is

$$k^2\phi(k) + a f_\lambda(k) \int \mathrm{d}^3k'\, f_\lambda(k')\phi(k') = -\kappa_\infty^2 \phi(k)\,. \tag{7}$$

1. Exact extrapolation formula

Let us assume now that we are in a limited model space with an effective sharp momentum cutoff Λ. In Sec. II we have illustrated how this cutoff is related to the truncation parameter of a finite HO basis; below we use a model interaction to further demonstrate the result $\Lambda = \Lambda_2$ numerically.

[2] $\phi(k)$ is the full three-dimensional wavefunction of the state, but it only depends on $k = |\mathbf{k}|$ due to the S-wave nature of the state, and we have absorbed the constant factor $Y_{00} = 1/\sqrt{4\pi}$ into the definition of ϕ.

Given Λ and defining $\phi_\Lambda(k) \equiv \phi(k)\Theta(\Lambda - k)$, Eq. (7) becomes

$$k^2\,\phi_\Lambda(k) + a\, f_\lambda(k)\,\Theta(\Lambda - k) \int \mathrm{d}^3k'\, f_\lambda(k')\,\phi_\Lambda(k') = -\kappa_\Lambda^2 \phi_\Lambda(k)\,. \tag{8}$$

Here, Θ denotes the unit step function, so $\Theta(\Lambda - k)$ is a projector, and Eq. (8) is obtained by simply introducing such a projector for each momentum dependence. To indicate the cutoff dependence of the energy eigenvalue, we now write it as $-\kappa_\Lambda^2$. Note that Eq. (8) turns into Eq. (7) for $\Lambda \to \infty$. We solve Eq. (8) for $\phi_\Lambda(k)$ and find (for $k < \Lambda$)

$$\phi_\Lambda(k) = \frac{c_\Lambda f_\lambda(k)}{\kappa_\Lambda^2 + k^2}\,, \tag{9}$$

where

$$c_\Lambda \equiv -a \int \mathrm{d}^3k\, f_\lambda(k)\,\phi_\Lambda(k) \tag{10}$$

is independent of k. Thus, we know the full momentum dependence of ϕ_Λ from Eq. (9). The cutoff does not imply that $\phi_\Lambda(k)$ goes smoothly to 0 at $k = \Lambda$, unlike the behavior of a coordinate-space wavefunction with a hard-wall boundary condition, because the momentum-space potential is nonlocal.

For determination of the eigenvalue κ_Λ we insert the solution (9) into Eq. (8)—or just substitute (9) into (10) and cancel the common factor c_Λ—to find the quantization condition

$$-1 = a \int \mathrm{d}^3k\, \frac{f_\lambda^2(k)\Theta(\Lambda - k)}{\kappa_\Lambda^2 + k^2} = 4\pi a \int_0^\Lambda \mathrm{d}k\, \frac{k^2\, f_\lambda^2(k)}{\kappa_\Lambda^2 + k^2}\,, \tag{11}$$

which is straightforward to solve numerically. Note that Eq. (11) implies that there is at most one bound state, as we have assumed. Note also that the quantized solution κ_Λ^2 *increases* to κ_∞^2 as Λ approaches ∞.

To derive an analytic formula for the dependence of κ_Λ on Λ, we start by defining (recall that we set $\hbar = 2\mu = 1$)

$$\Delta E_\Lambda \equiv E_\Lambda - E_\infty = \kappa_\infty^2 - \kappa_\Lambda^2\,. \tag{12}$$

Inserting this into Eq. (11) and Taylor-expanding to first order in $\Delta E_\Lambda/\kappa_\infty^2$, we find

$$\begin{aligned} -1 &= a \int \mathrm{d}^3k\, \frac{f_\lambda^2(k)\Theta(\Lambda - k)}{\kappa_\infty^2 + k^2 - \Delta E_\Lambda} \\ &\approx a \int \mathrm{d}^3k\, \frac{f_\lambda^2(k)\Theta(\Lambda - k)}{\kappa_\infty^2 + k^2} \left(1 + \frac{\Delta E_\Lambda}{\kappa_\infty^2 + k^2}\right) \\ &= -1 - a \int \mathrm{d}^3k\, \frac{f_\lambda^2(k)\Theta(k - \Lambda)}{\kappa_\infty^2 + k^2} \\ &\quad + \Delta E_\Lambda\, a \int \mathrm{d}^3k\, \frac{f_\lambda^2(k)\Theta(\Lambda - k)}{(\kappa_\infty^2 + k^2)^2}\,. \end{aligned} \tag{13}$$

In the second step here we have employed Eq. (11) for $\Lambda = \infty$, also using $\Theta(\Lambda - k) = 1 - \Theta(k - \Lambda)$. Thus, the general result for ΔE_Λ is

$$\Delta E_\Lambda \approx \frac{\int \mathrm{d}^3k\, \frac{f_\lambda^2(k)\Theta(k-\Lambda)}{\kappa_\infty^2 + k^2}}{\int \mathrm{d}^3k\, \frac{f_\lambda^2(k)\Theta(\Lambda-k)}{(\kappa_\infty^2 + k^2)^2}}\,. \tag{14}$$

This should be a quantitatively accurate expression in those regions of Λ for which $\Delta E_\Lambda \le \kappa_\infty^2$.

We can further approximate the result by dropping terms of $\mathcal{O}(\kappa_\infty^2/\Lambda^2)$, noting that this may not be a good quantitative approximation when $\Lambda \approx \lambda$:

$$\begin{aligned}\Delta E_\Lambda &= \frac{\int \mathrm{d}^3k\, \frac{f_\lambda^2(k)\Theta(k-\Lambda)}{k^2}}{\int \mathrm{d}^3k\, \frac{f_\lambda^2(k)\Theta(\Lambda-k)}{(\kappa_\infty^2 + k^2)^2}}\Big[1 + \mathcal{O}(\kappa_\infty^2/\Lambda^2)\Big] \\ &\approx \frac{\int \mathrm{d}^3k\, \frac{f_\lambda^2(k)\Theta(k-\Lambda)}{k^2}}{\int \mathrm{d}^3k\, \frac{f_\lambda^2(k)}{(\kappa_\infty^2 + k^2)^2}}\Big[1 + \mathcal{O}(\kappa_\infty^2/\Lambda^2)\Big]\,. \end{aligned} \tag{15}$$

In the last step, we extended the integration in the denominator from Λ to ∞. This introduces a negligible error for reasonable regulators when $\Lambda \gg \lambda$. However, we may want to keep the Λ-dependence in the denominator more general.

If we make all these approximations, then the Λ-dependence of ΔE_Λ is simple, and we have

$$\Delta E_\Lambda \propto \int \mathrm{d}k\, f_\lambda^2(k)\Theta(k-\Lambda) = \int_\Lambda^\infty \mathrm{d}k\, f_\lambda^2(k)\,. \tag{16}$$

Thus, the cutoff dependence is determined entirely by the regulator, while the low-energy length scale a has dropped out in this approximation and only appears in weaker approximations through κ_∞. In other words, the energy correction will depend strongly on the details of how the potential falls off at high momentum, but only weakly on the strength of the potential.

2. Perturbation theory

Here we show that the result (15) for ΔE_Λ in the region $\Lambda > \lambda$ can also be derived from first-order perturbation theory. The unperturbed wavefunction is from Eq. (9) with $\Lambda \to \infty$:

$$\phi_\infty(k) \equiv \langle k|\phi_\infty\rangle = \frac{c_\infty f_\lambda(k)}{\kappa_\infty^2 + k^2}\,, \tag{17}$$

and the perturbation can be written (for S-waves) as

$$\begin{aligned}\delta H(k,k') = -\Big[&k^2 \frac{\delta(k-k')}{4\pi k k'}\Theta(k-\Lambda)\Theta(k'-\Lambda) \\ &+ a\, f_\lambda(k') f_\lambda(k)\big[\Theta(k-\Lambda) + \Theta(k'-\Lambda)\big]\Big]\,. \end{aligned} \tag{18}$$

In writing $\delta H(k,k')$, we have neglected a contribution to the second term proportional to $\Theta(k-\Lambda)\Theta(k'-\Lambda)$, which would be doubly suppressed by $f_\lambda(k > \Lambda)$.

The first-order energy shift is

$$\begin{aligned}\Delta E_\Lambda &= \frac{\langle\phi_\infty|\delta H|\phi_\infty\rangle}{\langle\phi_\infty|\phi_\infty\rangle} \\ &= -\Big[4\pi c_\infty^2 \int_\Lambda^\infty \mathrm{d}k\, k^2 \frac{k^2 f_\lambda^2(k)}{(\kappa_\infty^2 + k^2)^2} \\ &\qquad + (2a) 4\pi c_\infty \int_0^\infty \mathrm{d}k'\, k'^2 f_\lambda(k') \frac{f_\lambda(k')}{\kappa_\infty^2 + k'^2} \\ &\qquad \times 4\pi c_\infty \int_\Lambda^\infty \mathrm{d}k\, k^2 f_\lambda(k) \frac{f_\lambda(k)}{\kappa_\infty^2 + k^2}\Big] \\ &\qquad \times \left[4\pi c_\infty^2 \int_0^\infty \mathrm{d}k\, k^2 \frac{f_\lambda^2(k)}{(\kappa_\infty^2 + k^2)^2}\right]^{-1} \\ &= -\left[\int_\Lambda^\infty \mathrm{d}k\, \frac{k^4 f_\lambda^2(k)}{(\kappa_\infty^2 + k^2)^2} - 2\int_\Lambda^\infty \mathrm{d}k\, \frac{k^2 f_\lambda^2(k)}{\kappa_\infty^2 + k^2}\right] \\ &\qquad \times \left[\int_0^\infty \mathrm{d}k\, \frac{k^2 f_\lambda^2(k)}{(\kappa_\infty^2 + k^2)^2}\right]^{-1} \\ &= \left[\int_\Lambda^\infty \mathrm{d}k\, f_\lambda^2(k)\right] \times \left[\int_0^\infty \mathrm{d}k\, \frac{k^2 f_\lambda^2(k)}{(\kappa_\infty^2 + k^2)^2}\right]^{-1} \\ &\qquad \times \Big[1 + \mathcal{O}(\kappa_\infty^2/\Lambda^2)\Big]\,. \end{aligned} \tag{19}$$

This agrees with Eq. (15) up to terms of order $\kappa_\infty^2/\Lambda^2$. Note that an analogous application of first-order perturbation theory fails if applied to the IR correction; one finds the leading $\mathrm{e}^{-2k_\infty L}$ dependence, but with the wrong coefficient.

3. Asymptotic expansion

It is instructive to look at the large Λ expansion of Eq. (16) when $f_\lambda(k)$ has the form of a Gaussian or super-Gaussian:

$$f_\lambda(k) = \mathrm{e}^{-(k/\lambda)^{2n}}\,. \tag{20}$$

We can express ΔE_Λ in this case in terms of the incomplete gamma function $\Gamma(a,z)$ [14]:

$$\begin{aligned}\Delta E_\Lambda &\propto \int_\Lambda^\infty \mathrm{d}k\, \mathrm{e}^{-2(k/\lambda)^{2n}} \\ &= \frac{\lambda}{4n}\int_{2(\Lambda/\lambda)^{2n}}^\infty \mathrm{d}t\, (t/2)^{\frac{1}{2n}-1}\mathrm{e}^{-t} \\ &= \frac{\lambda}{4n}\frac{1}{2^{\frac{1}{2n}-1}}\Gamma\left(\frac{1}{2n}, 2(\Lambda/\lambda)^{2n}\right)\,, \end{aligned} \tag{21}$$

so that for $\Lambda \gg \lambda$,

$$\Delta E_\Lambda(\Lambda) \underset{\Lambda\gg\lambda}{\longrightarrow} [\text{const.}] \times \lambda \left(\frac{\Lambda}{\lambda}\right)^{1-2n} \mathrm{e}^{-2(\Lambda/\lambda)^{2n}}\,. \tag{22}$$

Only for $n = 1$ does this have the Gaussian form used in phenomenological methods for extrapolation, which is

further verification of the non-universality of UV corrections. However, the asymptotic region where $\Lambda \gg \lambda$ is seldom reached in practice (if it were, convergence would likely be sufficient without extrapolation). When Λ is the same size as or smaller than λ, and if the region over which a fit is made is limited, then a Gaussian form can arise, as shown in Sec. IV B.

4. Numerical calculations

We test the extrapolation law (16) with the specific but arbitrary choice

$$f_\lambda(k) = \mathrm{e}^{-(k/\lambda)^4}\,, \tag{23}$$

with $\lambda = 2.0$ fm^{-1} and $a = -0.1$ fm. The solution of the quantization condition (11) yields $\kappa_\infty \approx 0.634$ fm^{-1}.

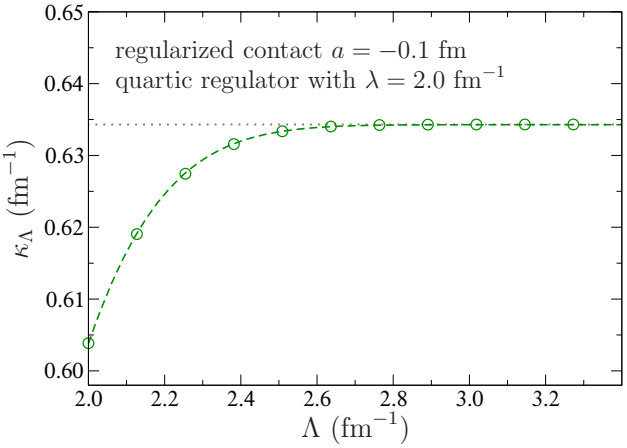

FIG. 5. (Color online) Test of the extrapolation law (16) for a contact $a = -0.1$ fm and the quartic regulator (23) with $\lambda = 2$ fm. Points: solution of the quantization condition (11). Line: fit of κ_∞ and A from Eq. (25).

Figure 5 shows the numerical solution of the exact quantization condition (11) plotted as κ_Λ *vs.* Λ (circles). The line is the extrapolation with the function (16), *i.e.*, we write

$$\Delta E_\Lambda = \kappa_\Lambda^2 - \kappa_\infty^2 \approx 2\kappa_\infty \Delta\kappa_\Lambda \;\text{ with }\; \Delta\kappa_\Lambda = \kappa_\infty - \kappa_\Lambda \tag{24}$$

and determine κ_∞ and the proportionality constant A from a fit to

$$\kappa_\Lambda = \kappa_\infty - \Delta\kappa = \kappa_\infty - A\int_\Lambda^\infty \mathrm{d}k\, f_\lambda^2(k)\,. \tag{25}$$

Note that $\kappa_\infty \ll \Lambda$, and $\Lambda > \lambda$, as required. Despite the approximations, the fit is very good, and in fact the extracted value for A agrees to better than 10% with the explicit result

$$A_\infty = \left(2\kappa_\infty \times \int_0^\infty \mathrm{d}k\, k^2 \frac{f_\lambda(k)^2}{(\kappa_\infty^2 + k^2)^2}\right)^{-1}\,, \tag{26}$$

which follows directly from combining Eqs. (15) and (24). This simple test already suggests that the approximations in deriving the extrapolation law (16) are well under control.

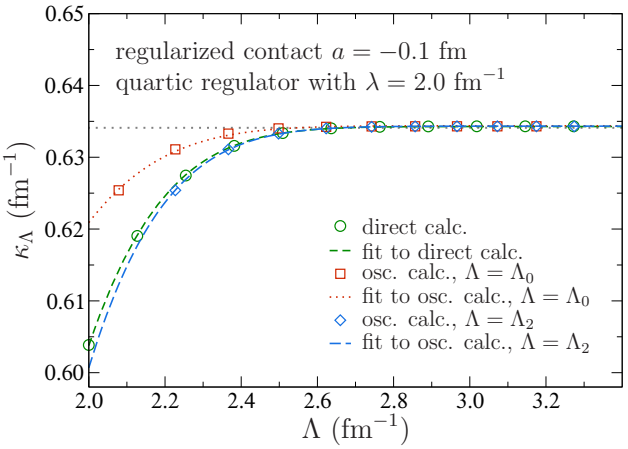

FIG. 6. (Color online) Oscillator calculations (with $b = 2.5$ fm and $n = 6, \ldots, 16$) and extrapolations for a contact $a = -0.1$ fm and quartic regulator (23) with $\lambda = 2$ fm. Circles and short-dashed line: direct-quantization result and fit, as in Fig. 5. Squares: oscillator result with $\Lambda = \Lambda_0(n)$. Dotted line: fit of Eq. (25) to squares. Diamonds: oscillator result with $\Lambda = \Lambda_2(n)$. Long-dashed line: fit of Eq. (25) to diamonds.

Indeed, the extrapolation also works very well for calculations in truncated oscillator bases, provided the effective UV cutoff is calculated according to $\Lambda = \Lambda_2$ as derived in Sec. II. Although the overall cutoff dependence is quite small for the simple regularized contact interaction, one can clearly see a substantial improvement when one uses $\Lambda = \Lambda_2$ instead of the naive estimate $\Lambda = \Lambda_0$. As shown in Fig. 6, the difference between the two choices is a horizontal shift of the oscillator data that moves them almost right on top of the direct-quantization result according to Eq. (11). If instead of Eq. (23) we use a Gaussian regulator,

$$f_\lambda(k) = \mathrm{e}^{-(k/\lambda)^2}\,, \tag{27}$$

the overall cutoff dependence is somewhat stronger, but, as shown in Fig. 7, the qualitative behavior is exactly the same. In fact, the agreement is even somewhat better, at least for the parameters chosen in the calculation.

To get a more quantitative assessment of the agreement, in Figs. 8 and 9 we plot the quantity

$$\Delta\kappa_\Lambda = |\kappa(m) - \kappa_{\Lambda(m)}| \tag{28}$$

on a logarithmic scale for different choices of Λ_m. With this notation we mean that for a given truncation parameter m we first calculate the corresponding effective cutoff Λ_m and then apply Eq. (11) to obtain the exact binding momentum for that cutoff. In these calculations we have used a very large oscillator length $b = 6.0$ fm to suppress IR corrections and go up to very large truncation parameters (up to $n = 72$) to still reach sizable UV

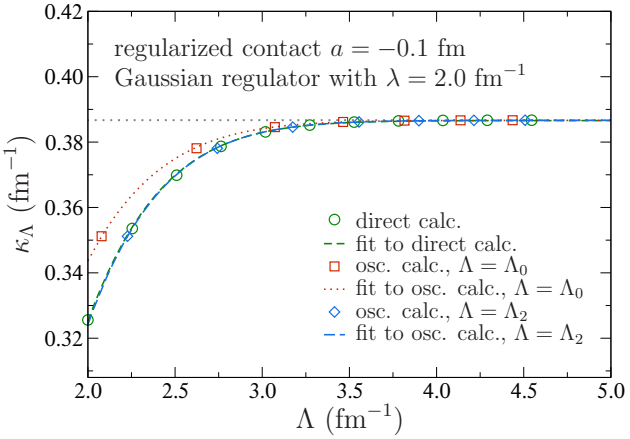
regularized contact $a = -0.1$ fm
Gaussian regulator with $\lambda = 2.0$ fm^{-1}
direct calc.
fit to direct calc.
osc. calc., $\Lambda = \Lambda_0$
fit to osc. calc., $\Lambda = \Lambda_0$
osc. calc., $\Lambda = \Lambda_2$
fit to osc. calc., $\Lambda = \Lambda_2$
κ_Λ (fm^{-1})
Λ (fm^{-1})

FIG. 7. (Color online) Oscillator calculations (with $b = 2.5$ fm and $n = 6, \ldots, 34$) and extrapolations for a contact $a = -0.1$ fm and Gaussian regulator (27) with $\lambda = 2$ fm. Symbols and curves are as in Fig. 6.

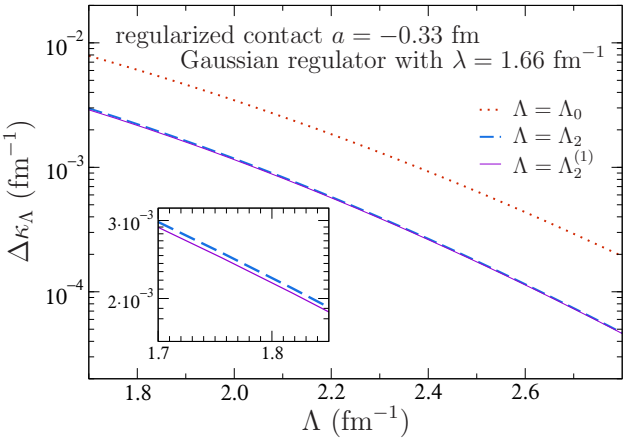

FIG. 9. (Color online) Logarithmic plot of $\Delta\kappa_\Lambda$ as defined in Eq. (28) for a contact $a = -0.33$ fm and Gaussian regulator (27) with $\lambda = 1.66$ fm. Curves and inset are as in Fig. 8.

cutoffs. For both regulators discussed above (quartic and Gaussian), the $\Lambda = \Lambda_2$ curve clearly lies below the one for $\Lambda = \Lambda_0$.

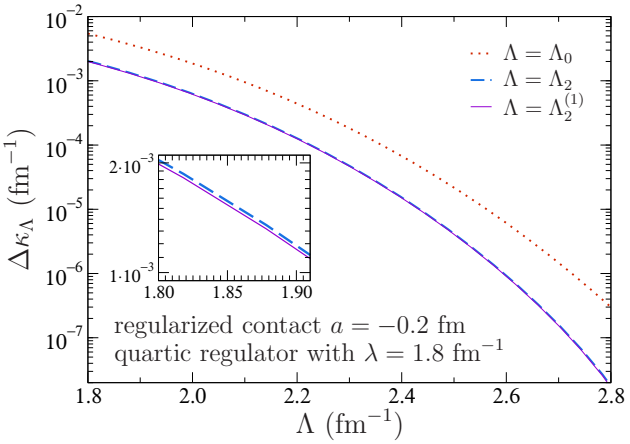

FIG. 8. (Color online) Logarithmic plot of $\Delta\kappa_\Lambda$ as defined in Eq. (28) for a contact $a = -0.2$ fm and quartic regulator (23) with $\lambda = 1.8$ fm. Dotted line: result for $\Lambda = \Lambda_0$. Thick dashed line: result for $\Lambda = \Lambda_2$. Thin dashed line: result for $\Lambda = \Lambda_2^{(1)}$ (including the first subleading correction). Inset: The small improvement from Λ_2 to $\Lambda_2^{(1)}$.

In these plots we have also included the result with the first subleading correction to $\Lambda = \Lambda_2$ (see Appendix A). It is reassuring to see that there is some small improvement (the curves for $\Lambda = \Lambda_2^{(1)}$ lie consistently below those for $\Lambda = \Lambda_2$), but we conclude that these corrections can safely be neglected for all present practical purposes.

B. Separable approximations

For a general rank-1 separable potential

$$\hat{V}_{\rm sep} = g\,|\eta\rangle\langle\eta|\,, \tag{29}$$

which in momentum space simply becomes (with $\eta(k) \equiv \langle k|\eta\rangle$)

$$V_{\rm sep}(k,k') = g\,\eta(k)\eta(k')\,, \tag{30}$$

the quantization condition (11) can be written as

$$-1 = 4\pi g \int_0^\Lambda {\rm d}k\, k^2 \frac{\eta(k)^2}{\kappa_\Lambda^2 + k^2}\,. \tag{31}$$

This is, of course, merely a change of notation, $a \to g$ and $f_\lambda(k) \to \eta(k)$ compared to Eq. (11). Most interactions used in practical calculations, however, do not have this convenient simple form (at least not in nuclear physics). Still, Eq. (31) can be put to some use.

Methods to obtain separable approximations for a given potential have been known and used for quite a while (see, *e.g.*, Refs. [10, 15, 16] and further references therein). We use the technique here in its simplest form, also called the *unitary pole approximation (UPA)* [10, 17]. Assuming that for an arbitrary potential $\hat{V}$ we know a (bound) eigenstate $|\psi\rangle$, we can construct a rank-1 separable approximation in momentum space by setting

$$\hat{V}_{\rm sep} = \frac{\hat{V}|\psi\rangle\langle\psi|\hat{V}}{\langle\psi|\hat{V}|\psi\rangle}\,. \tag{32}$$

In other words, we have

$$\eta(k) = \langle k|\hat{V}|\psi\rangle \tag{33}$$

for the momentum-space "form factor," and the coupling strength $g = \langle\psi|\hat{V}|\psi\rangle$ is, of course, independent of any

particular representation. From Eq. (32) one immediately sees that

$$\hat{V}_{\rm sep}|\psi\rangle = \hat{V}|\psi\rangle\,. \tag{34}$$

This means that the separable approximation is constructed in such a way that it exactly reproduces the state $|\psi\rangle$ used for its construction. The potential (32) reproduces the exact half off-shell T-matrix at the energy corresponding to the state ψ, and more sophisticated approximations (separable potential of rank > 1) can be constructed by using more than a single state [10]. Since we are only interested in performing the UV extrapolation for a single state here, however, the rank-1 approximation should be sufficient. In fact, based on our expectation that the UV extrapolation we seek should depend on short-range/high-momentum modes of the potential and the state under consideration, Eq. (32) looks very promising. To assess to what extent it actually reflects the UV behavior of a calculation based on the *original* potential, we first consider some examples where the separable approximation can be constructed analytically.

a. Spherical well. One of the simplest potentials for which the bound-state wavefunctions can be written down explicitly in closed form is the spherical well (step),

$$V_{\rm step}(r) = V_0\,\Theta(R-r) \quad , \quad V_0 < 0\,. \tag{35}$$

The eigenfunctions for this standard textbook example are spherical Bessel functions. Separable approximations for these potential have been discussed in Ref. [18]. If $V_{\rm step}$ supports an S-wave bound-state at energy $E=-\kappa^2$, we find from the results presented there that

$$\eta_{\rm step}(k) = \frac{2}{\pi}V_0R^2\frac{Z(E;V_0,kR)}{K^2-k^2}\,, \tag{36a}$$

$$g_{\rm step} = \left(\frac{2}{\pi}V_0R^2\,F(E;V_0,R)\right)^{-1}\,, \tag{36b}$$

with $K\equiv K(E;V_0)=\sqrt{E-V_0}$ and

$$L(E;V_0,R) = K\,\frac{j_0'(KR)}{j_0(KR)}\,, \tag{37}$$

$$Z(E;V_0,kR) = k\,j_0'(KR) - L(E;V_0,R)\,j_0(KR)\,, \tag{38}$$

$$F(E;V_0,R) = \frac{1}{2KR}\Big[R^2L(E;V_0,R) + RL(E;V_0,R) + R^2K\Big]\,. \tag{39}$$

In Fig. 10 we show how the separable approximation (36) (squares) performs compared to the original potential (35) (circles) in an oscillator calculation. We use $V_0=-4$ fm^{-1} and $R=1$ fm, which produces a bound state at $\kappa_\infty\approx 0.638$ fm^{-1} (determined numerically from the quantization condition for attractive step potentials and shown as the dotted line in Fig. 10). The dashed line furthermore shows the result of a direct calculation based on Eqs. (31) and (36) (see inset).

The results of all three calculations agree remarkably well. The fact that the separable approximation used in the oscillator calculations follows the result from the direct quantization according to Eq. (31) is primarily reassuring. More interestingly, the latter also traces the result of a "full" oscillator calculation based on the original step potential—including the rather slow convergence towards the exact result and even the peculiar step around $\Lambda\approx 6$ fm^{-1} in Fig. 10.

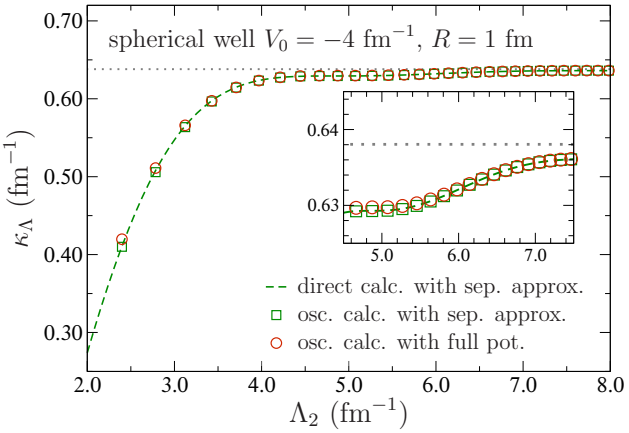

FIG. 10. (Color online) Oscillator calculations (with $b=2.0$ fm and $n=4,\ldots,64$) for a spherical step potential with $V_0=-4$ fm^{-1} and $R=1$ fm and its separable approximation. Dashed line: direct-quantization result according to Eqs. 31 and (36). Squares: oscillator result with separable approximation (36). Circles: oscillator result with the original (full) potential (35). The horizontal dotted line indicates the exact result for the binding momentum.

These features are due to the rather pathological (oscillatory) behavior of the step potential in momentum space. In the next subsection, we avoid this complication by studying another class of exactly solvable interactions, which are smooth.

b. Pöschl–Teller potential. It is convenient for us to consider a so-called Pöschl–Teller potential of the form

$$V_{\rm PT}(r) = -\frac{\alpha^2\beta(\beta-1)}{\cosh^2(\alpha r)} \tag{40}$$

Originally, this potential describes a one-dimensional problem on the interval $(-\infty,\infty)$. However, restricting ourselves to S-waves (and to states with odd wavefunctions), we can use it as a solvable problem in three dimensions. For given values of α and β, this potential has an analytically known bound-state spectrum. Labeling different states by an index ν, we have, for example, a single bound state ($\nu=0$) with binding momentum $\kappa=\alpha$ for $\beta=3$. For $\beta=5$, there are two bound states at $\kappa=3\alpha$ ($\nu=0$) and $\kappa=\alpha$ ($\nu=1$). The wavefunctions for this potentials are known analytically as well, which allows us to derive explicit expressions for the form factors $\eta(k)$ as well. These details are given in Appendix B.

In Fig. 11 we show results for a Pöschl–Teller potential with $\beta=3$ and a bound-state at $\kappa=\alpha=2/3$ fm^{-1}. The curves are analogous to those shown in Fig. 10 for

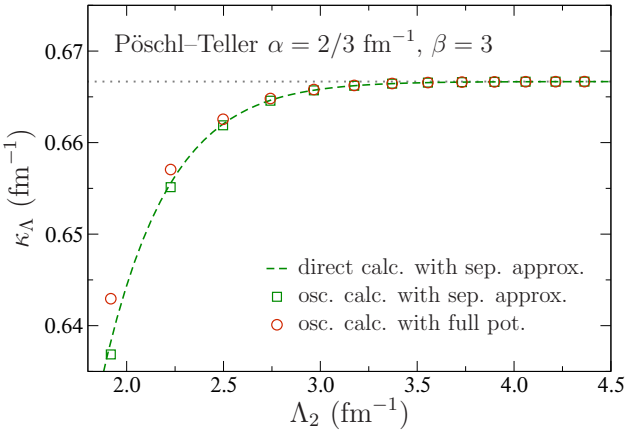

FIG. 11. (Color online) Oscillator calculations (with $b = 2.5$ fm and $n = 4, \ldots, 32$) for a Pöschl–Teller potential with $\beta = 3$ and $\alpha = 2/3$ fm^{-1} and its separable approximation. Dashed line: direct-quantization result according to Eqs. 31 and (B3). Squares: oscillator result with separable approximation (B3). Circles: oscillator result with the original (full) potential (40). The horizontal dotted line indicates the exact result for the binding momentum.

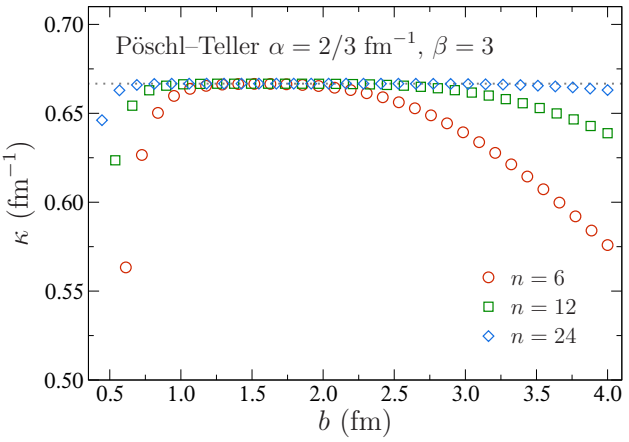

FIG. 12. (Color online) Binding momentum as a function of b obtained from oscillator with different basis sizes. Circles: $n = 6$. Boxes: $n = 12$. Diamonds: $n = 24$. The horizontal dotted line indicates the exact result for the binding momentum.

the step potential. While the agreement of the calculations with the original potential and with the separable approximation is not as impressive as for the step potential, it is still very good for cutoffs $\Lambda_2 \gtrsim 2.5$ fm^{-1} ($n > 8$).

In general, the regime where UV cutoff effects dominate the energy correction can be found from plots like the one shown in Fig. 12, where we plot the b-dependence of κ for our Pöschl–Teller potential with $\beta = 3$ and $\alpha = 2/3$ fm. Recalling that large b correspond to large configuration-space boxes $L_2 = \sqrt{2(2n + 3/2 + 2)}b$ and thus negligible IR correction, we identify the UV-dominated region as the one with $b \gtrsim 2$.

C. UV extrapolation for Pöschl-Teller potential

Based on these encouraging results, we now turn to actual extrapolations. The simplest fit formula one can write down for that purpose is

$$\text{(fit ``}\eta\text{'')} \qquad \kappa_\Lambda = \kappa_\infty - A \int_\Lambda^\infty \mathrm{d}k\, \eta(k)^2 \,, \tag{41}$$

which is just Eq. (25) in a more general notation ($f_\lambda \to \eta$). In the absence of an explicit scale λ associated with the separable "form factor," however, it is not *a priori* clear that the various approximations made in Sec. III A are rigorously justified. Without any of those approximations, the most general fit formula—based directly on Eq. (14)—is

$$\text{(fit ``}\eta\text{, full'')} \qquad \kappa_\Lambda = \kappa_\infty - A \frac{\displaystyle\int_\Lambda^\infty \mathrm{d}k\, \frac{k^2\, \eta(k)^2}{\kappa_\infty^2 + k^2}}{\displaystyle\int_0^\Lambda \mathrm{d}k\, \frac{k^2\, \eta(k)^2}{(\kappa_\infty^2 + k^2)^2}} \,. \tag{42}$$

This is actually quite restrictive since for an exact calculation one would expect $A \approx 1/(2\kappa_\infty)$ here, and in a fit to the binding energies instead of the binding momenta one should expect a prefactor ~ 1. As one more alternative, one can choose a middle ground and write

$$\text{(fit ``}\eta'\text{'')} \qquad \kappa_\Lambda = \kappa_\infty - A \int_\Lambda^\infty \mathrm{d}k\, \frac{k^2\, \eta(k)^2}{\kappa_\infty^2 + k^2} \,, \tag{43}$$

which is obtained from Eq. (42) by extending the integral in the denominator up to infinity—rendering it independent of Λ—and then absorbing the whole term into the fit constant A. In the next section, we compare the three approaches to one another and to phenomenological fits (Gaussian, exponential).

Of course, we are ultimately interested in performing these fits for potentials for which we have no analytical knowledge of the wavefunctions. Fortunately, the diagonalization calculation in the truncated oscillator basis does provide us at least with approximate wavefunctions, so it is natural to simply use the "best" solution available[3] from a set of calculations, *i.e.*, set

$$\eta(k) = \langle k|\hat{V}|\psi\rangle_{\text{HO, best}} \tag{44}$$

in what can be called a "bootstrap extrapolation" because—aside from the original potential—it only uses information that comes out of the numerical calculation. If the interaction $\hat{V}$ is already given on a momentum-space mesh for the numerical calculation, Eq. (44) is very

[3] Typically, "best" would refer to the result from the largest available oscillator space and the most UV-converged (small b) calculation. In practice, one could also make several choices for the extrapolation and take the spread in the result as a lower bound for the fit uncertainty.

simple (and fast) to implement. Using that wavefunction, one can perform a direct extrapolation to $\Lambda \to \infty$ by simply using the corresponding $\eta(k)$ in the separable quantization condition (31) without fitting a range of data points. Below, we refer to this approach as "η, direct."

Possible phenomenological approaches for extrapolation fits include a simple exponential,

$$\text{(fit "}E\text{")} \qquad \kappa_\Lambda = \kappa_\infty - A\,\mathrm{e}^{-B\Lambda}\,, \tag{45}$$

or a Gaussian

$$\text{(fit "}G\text{")} \qquad \kappa_\Lambda = \kappa_\infty - A\,\mathrm{e}^{-B\Lambda^2}\,. \tag{46}$$

We now investigate how well our separable extrapolations perform in comparison to Eqs. (45) and (46). We point out that they are quite a bit more constrained because they use only two fit parameters (κ_∞ and A) instead of three (κ_∞, A, and B). As described above, we follow the bootstrap procedure and take the wavefunction from the "best" numerical calculation available to construct the $\eta(k)$ used for the extrapolation. Since we have analytical expressions for the wavefunctions, we additionally show the extrapolation results obtained with those. This allows us to get at least an idea of how much influence it has on the extrapolation if the wavefunction is only given in a truncated basis.

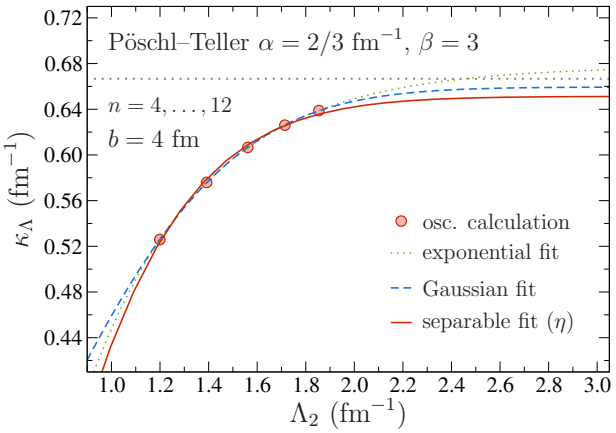

FIG. 13. (Color online) Comparison of UV extrapolations for an oscillator calculation (fixed $b = 4.0$ fm, running $n = 4, \ldots, 12$) with a $\beta = 3$, $\alpha = 2/3$ fm^{-1} Pöschl–Teller potential. Circles: oscillator results. Dotted line: exponential extrapolation (fit "E"). Dashed line: Gaussian extrapolation (fit "G"). Solid line: simplest separable extrapolation (fit "η"). The horizontal dotted line indicates the exact result for the binding momentum.

In Table I we give a detailed account of the results for a Pöschl–Teller potential with $\alpha = 2/3$ fm^{-1} and $\beta = 3$, which supports a single bound state with binding momentum $\kappa_{\infty,\text{exact}} = \alpha$. Comparison plots for the $n = 4, \ldots, 12$ and $b = 3.5, \ldots, 5.5$ fm datasets are shown in Figs. 13 and 14 respectively. To avoid cluttering, only the two phenomenological fits according to Eqs. (45) and (46) and the simplest separable one—Eq. (41) with $\eta(k)$ constructed from the numerical data—are shown in the figures. Table II furthermore shows a detailed comparison for the excited state (at $\kappa_{\infty,\text{exact}} = 1/3$ fm^{-1}) of a Pöschl–Teller potential with $\beta = 5$ and $\alpha = 1/3$ fm^{-1}.[4]

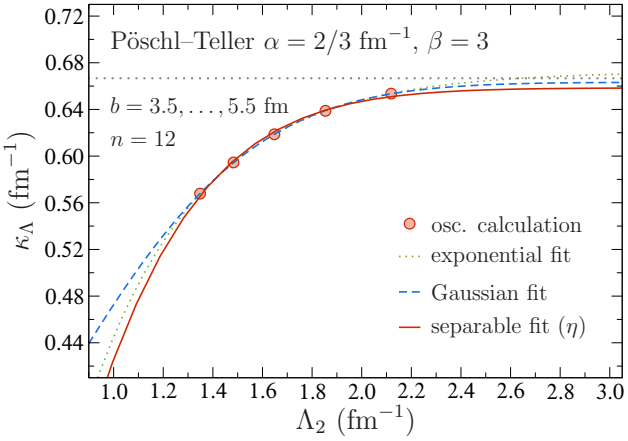

FIG. 14. (Color online) Same as Fig. 13, but now with fixed basis size $n = 12$ and running oscillator length $b = 3.5, \ldots, 5.5$ fm.

From the results presented in the tables and figures, we draw the following conclusions at this point:

- None of the fits produces the correct (exact) binding momentum right away, not even if the calculation is already converged to within only 2%. It should be noted, however, that we made no effort (*e.g.*, weighting) here to improve the fits. The only exception to this is the excited state of the $\beta = 5$ Pöschl–Teller potential (see Table II), where the Gaussian fit works remarkably well. This may be an accidental property of that potential and just supports our previous statement that in general it is desirable to have an extrapolation approach that really takes into account information from the particular potential and state under consideration.

- On average, the Gaussian fit mostly produces the best (closest to the exact answer) results. Except for the least-converged oscillator calculations, however, the separable fits based on our analytical knowledge of the exact wavefunctions work as well as the corresponding Gaussian ones. This indicates that the main limitation of the separable approach is the incomplete knowledge of the wavefunction that one gets from the numerical calculations.

- For the more converged calculations, however, the completely numerical separable fits come close to

[4] This potential has a deeper ground state with binding momentum $\kappa = 3\alpha = 1$ fm^{-1}.

TABLE I. Comparison of different extrapolations for a Pöschl–Teller potential with $\alpha = 2/3$ and $\beta = 3$. For calculations where n is varied, it is increased in steps of 2, and b is held fixed at 4.0 fm. For calculations with variable b (increasing in steps of 0.5 fm), n is held fixed at 12. The dimension of κ_∞ is always fm^{-1} and has been omitted in the table. Percentage values in parentheses give the relative difference, defined here as $100 \times (1 - |\kappa_\infty/\kappa_{\infty,\mathrm{exact}}|)$, of the extrapolated values to the exact answer $\kappa_{\infty,\mathrm{exact}} \approx 0.6667\ \mathrm{fm}^{-1}$.

V_{PT} with $\alpha = 2/3\ \mathrm{fm}^{-1}$, $\beta = 3 \ \rightarrow\ \kappa_{\infty,\mathrm{exact}} \approx 0.6667\ \mathrm{fm}^{-1}$					
Calculation	$n = 2$–8	$n = 4$–12	$n = 6$–16	$b = 4.5$–6.5 fm	$b = 3.5$–5.5 fm
$\kappa_{\Lambda_{\max}}$	0.607 (8.9%)	0.639 (4.2%)	0.6530 (2.04%)	0.619 (7.2%)	0.6535 (1.97%)
Phenomenological fits					
κ_∞, "E"	0.694 (4.1%)	0.678 (1.7%)	0.6719 (0.79%)	0.685 (2.8%)	0.6726 (0.89%)
κ_∞, "G"	0.650 (2.5%)	0.659 (1.2%)	0.6633 (0.51%)	0.656 (1.6%)	0.6633 (0.51%)
Separable fits with exact η					
κ_∞, "η"	0.651 (2.4%)	0.659 (1.2%)	0.6628 (0.59%)	0.655 (1.8%)	0.6620 (0.70%)
κ_∞, "η'"	0.661 (0.9%)	0.662 (0.7%)	0.6642 (0.38%)	0.660 (1.0%)	0.6635 (0.47%)
κ_∞, "η, full"	0.644 (3.4%)	0.658 (1.3%)	0.6631 (0.54%)	0.653 (2.1%)	0.6622 (0.67%)
Separable fits with η from best oscillator calculation					
κ_∞, "η"	0.633 (5.1%)	0.651 (2.4%)	0.6593 (1.11%)	0.642 (3.7%)	0.6585 (1.23%)
κ_∞, "η'"	0.639 (4.2%)	0.654 (1.9%)	0.6604 (0.94%)	0.646 (3.1%)	0.6598 (1.03%)
κ_∞, "η, full"	0.630 (5.5%)	0.651 (2.4%)	0.6596 (1.06%)	0.641 (3.9%)	0.6587 (1.19%)
Direct quantization with η from best oscillator calculation					
κ_∞, "η, direct"	0.652 (2.2%)	0.661 (0.9%)	0.6643 (0.36%)	0.655 (1.8%)	0.6644 (0.35%)

TABLE II. Comparison of different extrapolations for a Pöschl–Teller potential with $\alpha = 1/3$ and $\beta = 5$. For calculations where n is varied, it is increased in steps of 2, and b is held fixed at 4.5 fm. For calculations with variable b (increasing in steps of 0.5 fm), n is held fixed at 16. See Table I and text for further explanation.

Excited state of V_{PT} with $\alpha = 2/3\ \mathrm{fm}^{-1}$, $\beta = 5 \ \rightarrow\ \kappa_{\infty,\mathrm{exact}} \approx 0.3333\ \mathrm{fm}^{-1}$					
Calculation	$n = 4$–12	$n = 6$–16	$n = 8$–18	$b = 5.5$–7.5 fm	$b = 4.5$–6.5 fm
$\kappa_{\Lambda_{\max}}$	0.313 (6.1%)	0.326 (2.2%)	0.3223 (3.31%)	0.301 (9.7)%)	0.3264 (2.08%)
Phenomenological fits					
κ_∞, "E"	0.348 (4.4%)	0.340 (2.0%)	0.3421 (2.63%)	0.357 (7.1%)	0.3394 (1.82%)
κ_∞, "G"	0.332 (0.4%)	0.334 (0.2%)	0.3341 (0.23%)	0.335 (0.5%)	0.3339 (0.17%)
Separable fits with exact η					
κ_∞, "η"	0.328 (1.6%)	0.330 (1.0%)	0.3287 (1.39%)	0.324 (2.8%)	0.3297 (1.09%)
κ_∞, "η'"	0.328 (1.6%)	0.330 (1.0%)	0.3291 (1.27%)	0.325 (2.5%)	0.3300 (1.00%)
κ_∞, "η, full"	0.325 (2.5%)	0.329 (1.3%)	0.3282 (1.54%)	0.322 (3.4%)	0.3294 (1.18%)
Separable fits with η from best oscillator calculation					
κ_∞, "η"	0.317 (4.9%)	0.326 (2.2%)	0.3240 (2.80%)	0.310 (7.0%)	0.3267 (1.99%)
κ_∞, "η'"	0.318 (4.6%)	0.327 (1.9%)	0.3243 (2.71%)	0.310 (7.0%)	0.3269 (1.93%)
κ_∞, "η, full"	0.315 (5.5%)	0.326 (2.2%)	0.3237 (2.89%)	0.309 (7.3%)	0.3265 (2.05%)
Direct quantization with η from best oscillator calculation					
κ_∞, "η, direct"	0.327 (1.9%)	0.332 (0.4%)	0.3303 (0.91%)	0.322 (0.0%)	0.3316 (0.52%)

the Gaussian results—although, as we have pointed out, the latter approach uses one more fit parameter.

- Reassuringly, there is little scatter in the different separable fits, Eqs. (41), (42), and (43). Except for the most converged calculations, the fit based on Eq. (43) produces significantly better (in the above sense) results than the other two. Returning to the discussion in Sec. III C, this might indicate that the Eq. (41) is not rigorously justified, whereas Eq. (42) is too constraining to fit the whole range of data. While it may be tempting to thus suggest Eq. (43) as the optimal fit strategy, it is not clear that our speculation here is correct in general or even for the

specific potentials considered here. Since the overhead of the analysis is small compared to the original diagonalization, in practice it should be useful to perform all three fits and take the scatter as an indicator for the stability and/or uncertainty of the method.

- Finally, it is interesting to see that the "direct" extrapolation based on the separable quantization condition (31) is able to produce results quite close to the exact answer based on just a single oscillator calculation with fixed n and b.

D. Separable deuteron extrapolation

At this point, we finally turn to extrapolations for the deuteron bound state as it comes out from oscillator calculations with realistic nucleon–nucleon interactions. While for this simple system one can actually choose oscillator spaces which yield results converged so well that no extrapolation is actually necessary, it is still the most interesting two-body system we can look at here and provides a starting point for extrapolations of many-body calculations to be looked at in the future.

1. Separable deuteron potential

The deuteron is the bound state in the ${}^3S_1$–${}^3D_1$ coupled-channel system of the n–p interaction. We write this potential as

$$\hat{V}_{SD} = \begin{pmatrix} \hat{V}_{00} & \hat{V}_{02} \\ \hat{V}_{20} & \hat{V}_{22} \end{pmatrix} , \tag{47}$$

where $\hat{V}_{\ell\ell'}$ are the angular momentum components of a given realistic nucleon–nucleon potential (naturally, $\hat{V}_{20} = \hat{V}_{02}^\dagger$). For simplicity, we have omitted here the remaining quantum numbers and just note that for the deuteron one has $S = J = 1$ and $T = 0$, for the spin, total angular momentum, and isospin, respectively. If we now write the deuteron wavefunction found from the potential (47) as

$$|\psi_d\rangle = \begin{pmatrix} |\psi_0\rangle \\ |\psi_2\rangle \end{pmatrix} , \tag{48}$$

we can construct a separable potential of the form

$$\hat{V}_{SD,\text{sep}} = g \begin{pmatrix} |\eta_0\rangle\langle\eta_0| & |\eta_0\rangle\langle\eta_2| \\ |\eta_2\rangle\langle\eta_0| & |\eta_2\rangle\langle\eta_2| \end{pmatrix} = g \begin{pmatrix} |\eta_0\rangle \\ |\eta_2\rangle \end{pmatrix} \begin{pmatrix} \langle\eta_0| \\ \langle\eta_2| \end{pmatrix}^T \tag{49}$$

if we set

$$|\eta_0\rangle = \hat{V}_{00}|\psi_0\rangle + \hat{V}_{02}|\psi_2\rangle , \tag{50a}$$

$$|\eta_2\rangle = \hat{V}_{20}|\psi_0\rangle + \hat{V}_{22}|\psi_2\rangle , \tag{50b}$$

and

$$g = \left(\langle\psi_0|\hat{V}_{00}|\psi_0\rangle + \langle\psi_2|\hat{V}_{22}|\psi_2\rangle + 2\,\mathrm{Re}\,\langle\psi_0|\hat{V}_{02}|\psi_2\rangle \right)^{-1} . \tag{51}$$

2. Coupled-channel separable extrapolation

To derive the extrapolation formula for this coupled-channel separable potential, we start by writing the Schrödinger equation as

$$\begin{pmatrix} \hat{k}^2 & 0 \\ 0 & \hat{k}^2 \end{pmatrix} \begin{pmatrix} |\psi_0\rangle \\ |\psi_2\rangle \end{pmatrix} + \left[g \begin{pmatrix} |\eta_0\rangle \\ |\eta_2\rangle \end{pmatrix} \begin{pmatrix} \langle\eta_0| \\ \langle\eta_2| \end{pmatrix}^T \right] \begin{pmatrix} |\psi_0\rangle \\ |\psi_2\rangle \end{pmatrix} = -\kappa^2 \begin{pmatrix} |\psi_0\rangle \\ |\psi_2\rangle \end{pmatrix} . \tag{52}$$

Just as in the single-channel case (*cf.* Sec. III A), it is straightforward to solve as

$$\begin{pmatrix} |\psi_0\rangle \\ |\psi_2\rangle \end{pmatrix} = c_\infty \begin{pmatrix} \hat{k}^2 + \kappa^2 & 0 \\ 0 & \hat{k}^2 + \kappa^2 \end{pmatrix}^{-1} \begin{pmatrix} |\eta_0\rangle \\ |\eta_2\rangle \end{pmatrix} \tag{53}$$

with a constant

$$c_\infty = g \left[\langle\eta_0|\psi_0\rangle + \langle\eta_2|\psi_2\rangle \right] . \tag{54}$$

Noting that the operator inversion in Eq. (53) can be carried out for the two diagonal terms individually and inserting the result back into Eq. (52), we get

$$\left[\begin{pmatrix} 1 & 0 \\ 0 & 1 \end{pmatrix} + g \begin{pmatrix} \langle\eta_0|\left(\hat{k}^2 + \kappa^2\right)^{-1}|\eta_0\rangle & 0 \\ 0 & \langle\eta_2|\left(\hat{k}^2 + \kappa^2\right)^{-1}|\eta_2\rangle \end{pmatrix} \right] \times \begin{pmatrix} |\eta_0\rangle \\ |\eta_2\rangle \end{pmatrix} = 0 . \tag{55}$$

Finally, by multiplying from the left with $(\langle\eta_0|, \langle\eta_2|)$, we arrive at a simple quantization condition for the binding momentum κ, which in momentum space reads

$$-1 = 4\pi g \int_0^\infty \mathrm{d}k\, k^2\, \frac{\eta_0(k)^2 + \eta_2(k)^2}{\kappa_\infty^2 + k^2} . \tag{56}$$

Repeating the whole procedure with appropriate projection operators to enforce a momentum cutoff Λ, we find

$$-1 = 4\pi g \int_0^\Lambda \mathrm{d}k\, k^2\, \frac{\eta_0(k)^2 + \eta_2(k)^2}{\kappa_\Lambda^2 + k^2}\,. \tag{57}$$

This is just Eq. (31) with the replacement

$$\eta(k)^2 \longrightarrow \eta_0(k)^2 + \eta_2(k)^2\,, \tag{58}$$

so it is simple to read off the coupled-channel extrapolation formulas from Eqs. (41) to (43). For example, the analog of Eq. (41) is just

$$\kappa_\Lambda = \kappa_\infty - A \int_\Lambda^\infty \mathrm{d}k\, \left[\eta_0(k)^2 + \eta_2(k)^2\right]\,. \tag{59}$$

3. *Extrapolation results*

In Fig. 15 we show results obtained with the Entem–Machleidt N3LO (500 MeV cutoff) potential. For the interaction SRG-evolved down to a resolution scale $\lambda = 2.0$ fm^{-1} (left panel), the picture is similar to what we found for the Pöschl–Teller potential in Sec. III C. With the oscillator calculation (performed at fixed $\Omega = 4$ MeV $\to b \approx 4.55$ fm), the Gaussian fit actually yields the exact answer $\kappa_d = 45.702$ (for the given interaction) to within 0.01%. The separable fits, however, also work very well and give the right answer to within 0.15 to 0.55 percent. The simple exponential fit does not perform well at all in this case.

Seeing how *all three* curves actually fit the data points very well with negligible residuals, however, the "danger" of purely phenomenological extrapolations becomes quite evident. If one does not use a known answer as guideline—as clearly one should not in a completely rigorous approach—it would be hard to judge which fit should be trusted.

For the results based on the "bare" (unevolved) interaction Fig. 15, right panel), the situation is even more dramatic: in this case, both phenomenological approaches fail badly (based on comparing their results to the known answer), whereas the separable approximation still works remarkably well (better than 1% agreement with exact answer). This should finally serve to exhibit the true value of this physically motivated extrapolation approach.

We find the same situation also for other nucleon–nucleon interactions. As a further example, we show in Fig. 16 results for the Epelbaum *et al.* N3LO potential (550/600 MeV cutoff). For the SRG-evolved interaction we see an interesting feature at $\Lambda_2 \sim 2.0$ fm^{-1}. The curve for the separable fit has a "bump" structure around this cutoff, but it ends up almost exactly at the converged value. To prove that this is not a peculiar artifact of the separable fit, we show in Fig. 17 results for the same potential but up to larger cutoffs. To also demonstrate once more the validity of identifying $\Lambda_2 = \Lambda_2(N, \Omega)$ as the relevant UV cutoff, we use in this case data points obtained at fixed N and varying Ω for the fits. The data points from Fig. 16 are shown at the same time for comparison. The plot shows that the bump structure really is a feature that is in the oscillator data. We point out that the simple exponential and Gaussian fits shown for comparison cannot possibly capture this kind of behavior. We hence claim that the separable fit approach is superior to the phenomenological ones also for SRG-softened interactions (at least for fits over a large cutoff range, *cf.* the following section).

Finally, to look at one more NN potential, we show in Fig. 18 results for the Epelbaum *et al.* interaction at N2LO. Since the overall situation is the same, we focus in this case on assessing the stability of the separable fits alone. To this end, we show now fit curves for the three versions—Eqs. (41) to (43) with $\eta(k)^2 \to \eta_0(k)^2 + \eta_2(k)^2$—obtained from oscillator calculations with $n = 5, 7, 9$ (instead of using just the one with the largest n). Although the overall spread is remarkably small, we suggest this procedure in order to assess the stability of the fit. Since the band generated this way unfortunately does not cover the exact answer for this potential ($\kappa_\infty \approx 45.3$ MeV), it is clear that this obviously gives a lower bound on the overall theoretical uncertainty of the calculation. Note, however, that the best oscillator result shown in the plot is only converged to within about 20%. We also point out that the separable fits still perform better than the phenomenological ones (not shown in the plot).

IV. RE-EXAMINING SRG-BASED EXTRAPOLATIONS

In the preceding section we showed that the separable extrapolation applied to the deuteron worked very well for bare potentials and SRG-evolved potentials. In this section, we re-examine prior results in the literature for SRG interactions. These include the phenomenological result that a Gaussian ansatz for the UV correction,

$$\Delta E_\infty \propto \mathrm{e}^{-b_1 \Lambda_2^2}\,, \tag{60}$$

gives good fits with $b_1 \approx 4/\lambda^2$ at resolution scale λ [5, 11].[5]

A. Perturbation theory for SRG potentials

Here we reconsider evaluating the UV correction in perturbation theory as in Sec. III A 2, but instead of a

[5] Note that these earlier works used an oscillator parameter b defined with the nucleon mass rather than the reduced mass as used here. Thus the numerical values of the effective IR and UV cutoffs differ by a factor of $\sqrt{2}$ compared to the SRG results given here.

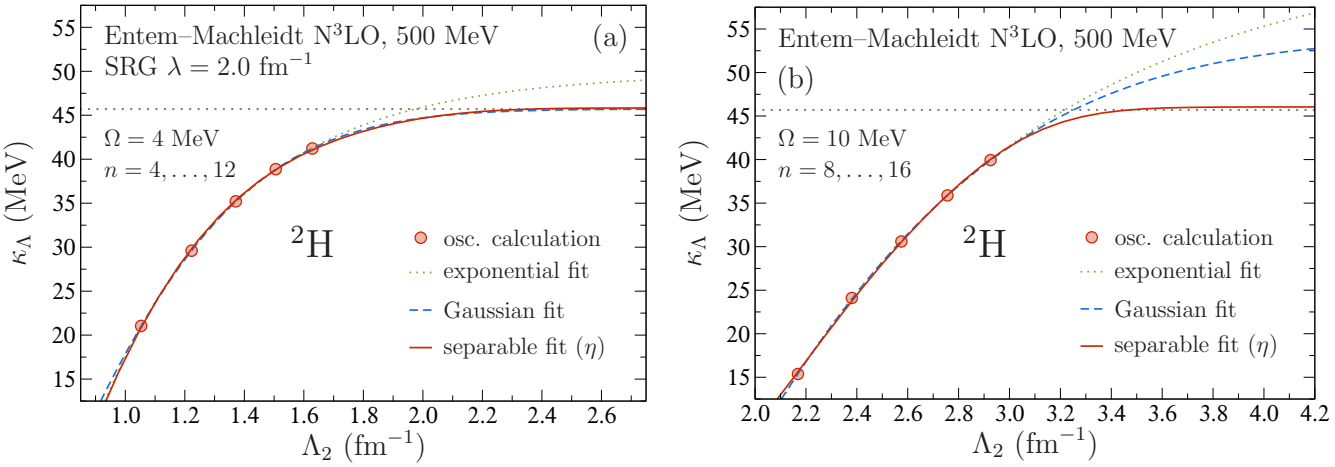

FIG. 15. (Color online) Comparison of UV extrapolations for a deuteron state calculated with the Entem–Machleidt N3LO (500 MeV cutoff) potential, (a) SRG-evolved down to a resolution scale $\lambda = 2.0$ fm^{-1} and (b) with the "bare" (unevolved) interaction. Circles: oscillator results. Dotted line: exponential extrapolation (fit "E"). Dashed line: Gaussian extrapolation (fit "G"). Solid line: simplest separable extrapolation (fit "η"). Dotted horizontal lines indicate the exact result for the binding momentum.

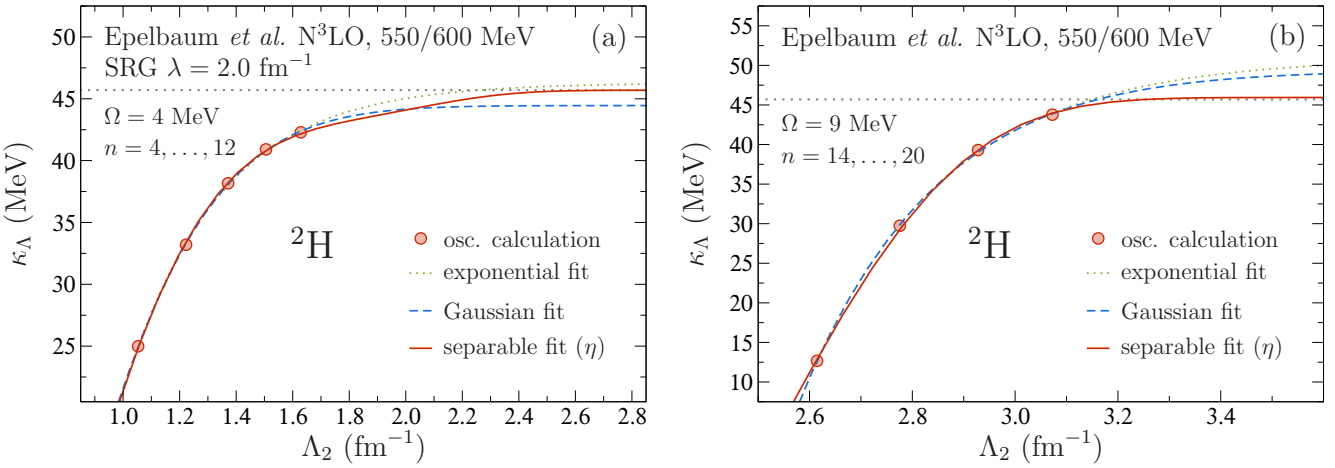

FIG. 16. (Color online) Comparison of UV extrapolations for a deuteron state calculated with the Epelbaum *et al.* N3LO (550/600 MeV cutoff) potential, (a) SRG-evolved down to a resolution scale $\lambda = 2.0$ fm^{-1} and (b) with the "bare" (unevolved) interaction. Symbols and curves are as in Fig. 16.

separable potential we only assume that we have a potential $V_\lambda(k,k')$ with a UV scale λ, the (dominant) behavior of which is known when one argument is small ($< \lambda$) and one argument is large ($> \lambda$). In particular, we expect the dominant dependence for SRG evolved potentials to be roughly [19, 20]

$$V_\lambda(k,k') \xrightarrow[k'\ll\lambda]{k>\lambda} V_\infty(k,k')\mathrm{e}^{-k^4/\lambda^4} \approx V_\infty(k,0)\mathrm{e}^{-k^4/\lambda^4}\,, \tag{61}$$

where $V_\infty(k,0)$ varies relatively slowly compared to $\mathrm{e}^{-k^4/\lambda^4}$ in the relevant range of k. Equation (61) follows from the SRG flow equations because of the dominance of the kinetic energy for far off-diagonal matrix elements (see Eq. (12) in Ref. [19]), together with an expansion about $k' = 0$. Another class of potentials with analogous behavior is the smooth $V_{\mathrm{low}\,k}$ potential with super-Gaussian regulators with a cutoff λ [21], for which the regulator dependence is strongly imposed on the potential.

The momentum space Schrödinger equation with $\Lambda = \infty$ is

$$k^2\phi_\infty(k) + \int \mathrm{d}^3k'\, V_\lambda(k,k')\phi_\infty(k') = -\kappa_\infty^2\phi_\infty(k)\,. \tag{62}$$

So the analog equation to (17) for the unperturbed wavefunction is

$$\phi_\infty(k) = \frac{-\int \mathrm{d}^3k'\, V_\lambda(k,k')\phi_\infty(k')}{k^2+\kappa_\infty^2}\,. \tag{63}$$

If we look at this wavefunction where $k > \lambda$, then we can take advantage of the integral being dominated by where

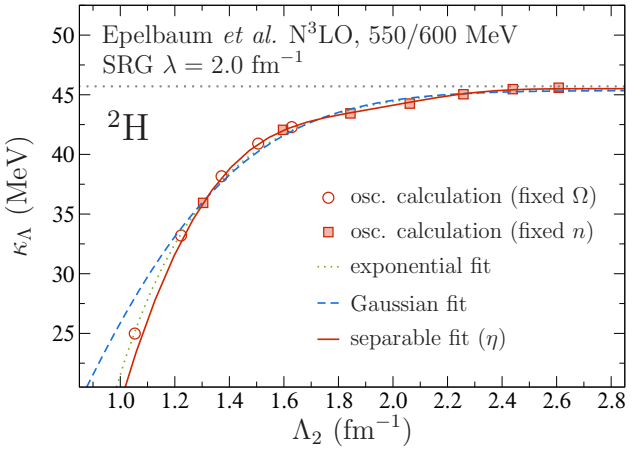

FIG. 17. (Color online) Comparison of UV extrapolations for a deuteron state calculated with the Epelbaum *et al.* N3LO (550/600 MeV cutoff) potential. Circles: oscillator results with fixed $\Omega = 4$ MeV and $n = 4, \ldots, 12$. Squares: oscillator results with fixed $n = 10$ and $\Omega = 3, \ldots, 12$ MeV (in steps of 1.5 MeV. Curves are as in Fig. 16 and show fits to the squares only.

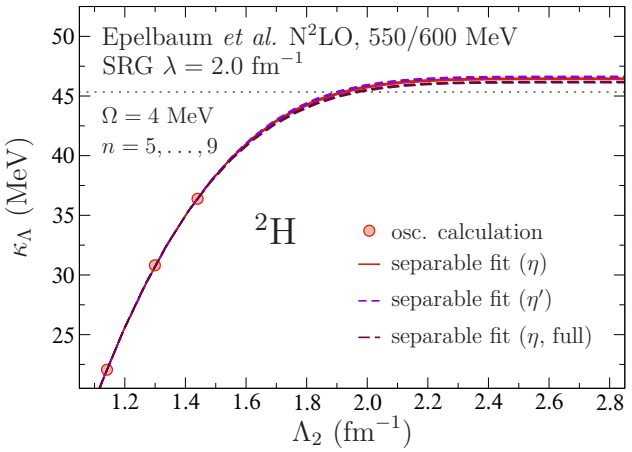

FIG. 18. (Color online) Comparison of UV extrapolations for a deuteron state calculated with the Epelbaum *et al.* N2LO (550/600 MeV cutoff) potential. Circles: oscillator results. Solid line: simplest separable extrapolation (fit "η"). Long-dashed line: general separable extrapolation (fit "η, gen."). Short-dashed line: modified general separable extrapolation (fit "η, gen.′"). The dotted horizontal line indicates the exact result for the binding momentum.

$\phi_\infty(k')$ is large, which is at low k', to expand $\widetilde{V}(k,k')$ about $k' = 0$ (here keeping only the leading term):

$$\phi_\infty(k) \xrightarrow{k>\lambda} -\frac{V_\lambda(k,0)}{k^2+\kappa_\infty^2}\int \mathrm{d}^3k'\,\phi_\infty(k')\,. \tag{64}$$

Given that the integration over the wavefunction is now a constant, and given Eq. (61) for $V_\lambda(k,0)$, which looks like $f_\lambda(k)$ (with some weaker k dependence), we see a close correspondence to the expression for the wavefunction in a pure separable potential given by $\phi(k)$ in Eq. (9).

The cutoff Hamiltonian is

$$H_\Lambda = \left[k^2\frac{\delta(k-k')}{kk'} + V_\lambda(k,k')\right]\Theta(\Lambda-k)\Theta(\Lambda-k')\,, \tag{65}$$

so the perturbation is $\delta H(k,k') = H_\Lambda - H_\infty$. Using $\Theta(\Lambda-k) = 1-\Theta(k-\Lambda)$, we find (*cf.* Eq. (18))

$$\delta H(k,k') = -\Bigg[k^2\frac{\delta(k-k')}{kk'}\Theta(k-\Lambda)\Theta(k'-\Lambda) + V_\lambda(k,k')[\Theta(k-\Lambda)+\Theta(k'-\Lambda)]\Bigg]\,. \tag{66}$$

The δ-function makes the second Θ function multiplying the kinetic energy redundant, while again we have dropped the $-\Theta(k-\Lambda)\Theta(k'-\Lambda)$ term. The first-order energy shift is

$$\begin{aligned}\Delta E_\infty &= \frac{\langle\phi_\infty|\delta H|\phi_\infty\rangle}{\langle\phi_\infty|\phi_\infty\rangle} \\ &= -\Bigg[\int_\Lambda^\infty \mathrm{d}k\,k^2\,k^2\phi_\infty^2(k) \\ &\qquad + 8\pi\int_0^\infty \mathrm{d}k'\,k'^2\int_\Lambda^\infty \mathrm{d}k\,k^2 \\ &\qquad\qquad \times \phi_\infty(k')V_\lambda(k',k)\phi_\infty(k)\Bigg] \\ &\qquad \times\left[\int_0^\infty \mathrm{d}k\,k^2\phi_\infty^2(k)\right]^{-1}\,.\end{aligned} \tag{67}$$

Now $\Lambda > \lambda$ in the present discussion, so we can apply Eq. (64) twice in the first (kinetic energy) integral and once in the second of the double integrals, also taking $V(k',k) \to V(0,k)$ at the same level of approximation:

$$\begin{aligned}\Delta E_\infty &\approx -4\pi\left[\int \mathrm{d}^3k'\,\phi_\infty(k')\right]^2\left[\int_\Lambda^\infty \mathrm{d}k\,\frac{k^4\,V_\lambda(0,k)V_\lambda(k,0)}{(\kappa_\infty^2+k^2)^2} - 2\int_\Lambda^\infty \mathrm{d}k\,\frac{k^2\,V_\lambda(0,k)V_\lambda(k,0)}{\kappa_\infty^2+k^2}\right]\times\left[\int_0^\infty \mathrm{d}^3k\,\phi_\infty^2(k)\right]^{-1} \\ &\approx 4\pi\frac{\left[\int \mathrm{d}^3k'\,\phi_\infty(k')\right]^2}{\left[\int \mathrm{d}^3k\,\phi_\infty^2(k)\right]}\times\left[\int_\Lambda^\infty \mathrm{d}k\,V_\lambda(0,k)V_\lambda(k,0)\right]\times\left[1+\mathcal{O}(\kappa_\infty^2/\Lambda^2)\right]\,.\end{aligned} \tag{68}$$

In the second line we have again just kept the leading term in $\kappa_\infty^2/\Lambda^2$, which lets us combine the integrals.

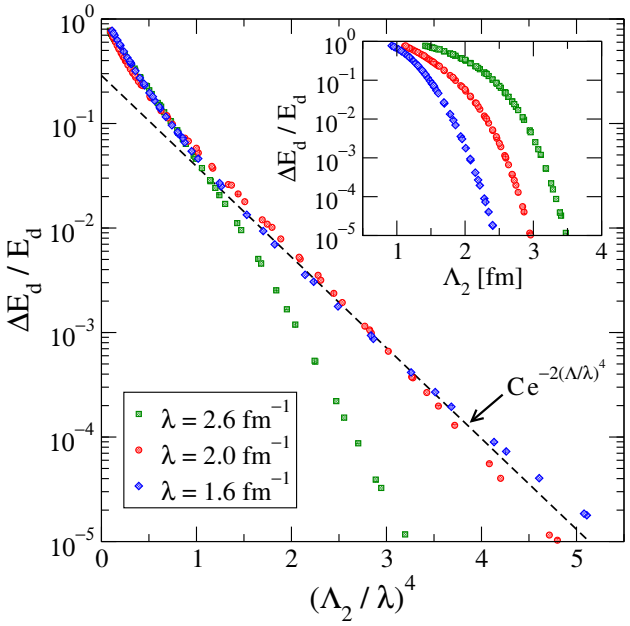

FIG. 19. (Color online) Relative error for the deuteron energy from HO basis truncation as a function of $(\Lambda_2/\lambda)^4$ for (N,Ω) values for which the IR correction can be neglected. Several SRG-evolved potentials are used, all with the same initial potential as in Fig. 15. The dashed line shows the expected slope (up to prefactors) for $\Lambda_2/\lambda \gg 1$ according to the analysis in Sec. III A 3. Inset: the relative error is plotted against the unscaled Λ_2.

Several observations can be made based on Eqs. (68) and (61). First, we have additional confirmation that the UV energy correction is not universal in the sense that unitarily equivalent potentials (such as SRG potentials at different λ values) will give different corrections, unlike the case for the IR correction (*e.g.*, see Fig. 21 in Ref. [7]). We see the same Λ dependence at this level as in the separable case. Therefore, the same analysis should apply when looking at the dependence of the energy correction in the asymptotic regime where $\Lambda > \lambda$. Note also that at LO (at least) we should find the correction is a function of Λ/λ. Both of these are consistent with numerical studies of the SRG-evolved deuteron energy in this regime with the SRG Hamiltonian cut off at $\Lambda > \lambda$. For example, in Fig. 19, the relative error in the deuteron is plotted as a function of $(\Lambda_2/\lambda)^4$ for SRG-evolved potentials ranging from $\lambda = 2.6\,\mathrm{fm}^{-1}$ to $\lambda = 1.6\,\mathrm{fm}^{-1}$. The inset shows how different the corrections are as a function of the *unscaled* Λ_2. When scaled, the errors largely coincide for $\Lambda_2 \le \lambda$ for all three potentials, but up to much higher cutoffs for the two lower values of λ (and for any λ below about $2.2\,\mathrm{fm}^{-1}$). Apparently a sufficient degree of evolution is needed to modify the high-momentum tail of the potential so that it follows the universal SRG asymptotic form for the correction ($\propto \mathrm{e}^{-2(\Lambda_2/\lambda)^4}$).

B. Gaussian ansatz for UV extrapolations

Based on the results in the last section, if we are in the asymptotic region where $\Lambda \gg \lambda$, we would not expect to find that the energy behaves like Eq. (60), but for SRG-evolved potentials roughly like $\mathrm{e}^{-2(\Lambda/\lambda)^4}$ times some slower-varying function of Λ. This is verified in Fig. 19. More generally the separable extrapolation has the form of an integral and not a simple functional form; so how might an approximate Gaussian dependence on Λ_2 arise?

The key is that in practice UV extrapolations have typically been applied in a *limited*, non-asymptotic region $\Lambda_{\min} < \Lambda < \Lambda_{\max}$ for which Λ/λ is about unity (*e.g.*, past NCSM fits were in the range $0.7 < \Lambda/\lambda < 1.1$ and the fit was primarily determined by the points at the lower end [5, 11]). While we expect ΔE_Λ to decrease rapidly with increasing Λ, $\log \Delta E_\Lambda$ should be well approximated by a low-order Taylor expansion in a small region. If ΔE_Λ is a function only of Λ^2 rather than Λ, then by keeping only through the linear term in the Λ^2 expansion we will have the phenomenological Gaussian ansatz for ΔE_Λ, with a prediction for b_1 possible from our separable expansion formalism.

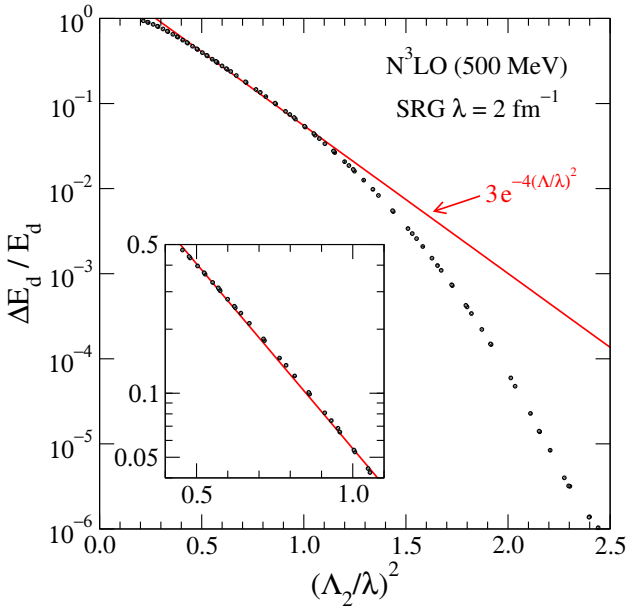

FIG. 20. (Color online) Relative error for the deuteron energy from HO basis truncation as a function of $(\Lambda_2/\lambda)^2$ for (N,Ω) values for which the IR correction can be neglected. The potential is the same as in Fig. 15. The solid line is an approximate fit to a region near $\Lambda_2/\lambda = 1$.

We first consider separable potentials and demonstrate that $\Delta E_\Lambda = \Delta E_\Lambda(\Lambda^2)$ for any $f_\lambda(k)$ that is a function of k^2. (For $\ell > 0$, we expect that $f_\lambda(k)$ will be of the form k^ℓ times a function of k^2, and the demonstration is trivially generalized.) We start with Eq. (14), which we expect to be quantitatively accurate in the region of interest. We first make the Λ dependence explicit in the

limits and then change variables to $u = k/\Lambda$:

$$\Delta E_\Lambda = \frac{\int \mathrm{d}^3k\, \frac{f_\lambda^2(k)\Theta(k-\Lambda)}{\kappa_\infty^2 + k^2}}{\int \mathrm{d}^3k\, \frac{f_\lambda^2(k)\Theta(\Lambda-k)}{(\kappa_\infty^2 + k^2)^2}} = \frac{\int_\Lambda^\infty \mathrm{d}k\, \frac{k^2 f_\lambda^2(k)}{\kappa_\infty^2 + k^2}}{\int_0^\Lambda \mathrm{d}k\, \frac{k^2 f_\lambda^2(k)}{(\kappa_\infty^2 + k^2)^2}}$$
$$= \frac{\int_1^\infty \mathrm{d}u\, \frac{u^2 f_\lambda^2(u\Lambda)}{\kappa_\infty^2/\Lambda^2 + u^2}}{\frac{1}{\Lambda^2}\int_0^1 \mathrm{d}u\, \frac{u^2 f_\lambda^2(u\Lambda)}{(\kappa_\infty^2/\Lambda^2 + u^2)^2}} . \qquad (69)$$

But by assumption $f_\lambda(u\Lambda)$ depends only on the argument squared and therefore only on Λ^2, so we have shown $\Delta E_\Lambda = \Delta E_\Lambda(\Lambda^2)$. Next we write:

$$g(\Lambda^2) \equiv \log \Delta E_\Lambda(\Lambda^2)$$
$$= \log \int_\Lambda^\infty \mathrm{d}k\, \frac{k^2 f_\lambda^2(k)}{\kappa_\infty^2 + k^2} - \log \int_0^\Lambda \mathrm{d}k\, \frac{k^2 f_\lambda^2(k)}{(\kappa_\infty^2 + k^2)^2} , \qquad (70)$$

and expand about $\Lambda^2 = \Lambda_*^2$,

$$g(\Lambda^2) = g_0 + g_1(\Lambda^2 - \Lambda_*^2) + \frac{1}{2}g_2(\Lambda^2 - \Lambda_*^2)^2 + \cdots . \qquad (71)$$

Truncating at the linear term, we obtain (with $b_1 = -g_1$)

$$\Delta E_\Lambda = [\mathrm{e}^{(g_0 - g_1\Lambda_*^2)}]\, \mathrm{e}^{g_1\Lambda^2} = (\text{const.}) \times \mathrm{e}^{-b_1\Lambda^2} , \qquad (72)$$

which is the Gaussian form we are looking for. We can directly evaluate the g_i for $i > 0$ using

$$\frac{\mathrm{d}}{\mathrm{d}\Lambda^2} = \frac{1}{2\Lambda}\frac{\mathrm{d}}{\mathrm{d}\Lambda} . \qquad (73)$$

Thus,

$$g_1 = \left.\frac{\mathrm{d}g}{\mathrm{d}\Lambda^2}\right|_{\Lambda_*^2}$$
$$= \frac{1}{2\Lambda_*}\left\{ \frac{-f_\lambda^2(\Lambda_*)\frac{\Lambda_*^2}{\kappa_\infty^2 + \Lambda_*^2}}{\int_{\Lambda_*}^\infty dk\, \frac{k^2 f_\lambda^2(k)}{\kappa_\infty^2 + k^2}} - \frac{f_\lambda^2(\Lambda_*)\frac{\Lambda_*^2}{(\kappa_\infty^2 + \Lambda_*^2)^2}}{\int_0^{\Lambda_*} \mathrm{d}k\, \frac{k^2 f_\lambda^2(k)}{(\kappa_\infty^2 + k^2)^2}} \right\} < 0 . \qquad (74)$$

Note that this is a negative-definite function of Λ_*^2 (*e.g.*, change variables again to $u = k/\Lambda_*$), so $b_1 > 0$. Finally, let us consider g_2. We need the second derivative of g:

$$\frac{\mathrm{d}}{\mathrm{d}\Lambda^2}\left(\frac{1}{\Delta E_\Lambda}\frac{\mathrm{d}\Delta E_\Lambda}{\mathrm{d}\Lambda^2}\right) = \frac{\mathrm{d}}{\mathrm{d}\Lambda^2}\left(\frac{\mathrm{d}\log \Delta E_\Lambda}{\mathrm{d}\Lambda^2}\right)$$
$$= -\frac{1}{\Delta E_\Lambda^2}\left(\frac{\mathrm{d}\Delta E_\Lambda}{\mathrm{d}\Lambda^2}\right)^2 + \frac{1}{\Delta E_\Lambda}\frac{\mathrm{d}^2\Delta E_\Lambda}{\mathrm{d}(\Lambda^2)^2} . \qquad (75)$$

Now the first term on the right-hand side of the last equality is negative definite. In the other term, $\Delta E_\Lambda(\Lambda^2)$ is positive definite and the curvature with respect to Λ^2 is positive. So we expect cancellation here for $\Lambda_* \approx \lambda$, which is verified numerically. With g_2 small, the linear approximation and therefore the Gaussian ansatz are valid. An example showing the Gaussian region for an SRG potential is given in Fig. 20, for which $b_1 = 4/\lambda^2$ is found to be a good fit, with $g_2 \approx 0$. This same value works with other light nuclei. Note that when fitting to the functional form $E(\Lambda) = E_\infty + B_0\mathrm{e}^{-b_1\Lambda^2}$, the choice of Λ_* is made implicitly by the fit to B_0 and b_1.

Let us briefly speculate why the Gaussian fit does not work well in general (see, *e.g.*, the right panel in Fig. 15 and both panels in 16). For the Gaussian fit to be applicable, g_2 needs to be sufficiently small that g_1 dominates for an accessible range of Λ. This condition is not met in general: Figure 21 shows the relative error of the deuteron binding energy as a function of $(\Lambda_2/\lambda)^2$, and the shaded regions indicate where the Gaussian fit was attempted (compare to Fig. 15). The condition that g_1 dominates means that $\Delta E_d/E_d$ is well approximated by a straight line, which is satisfied for the SRG-evolved potential (left shaded region) but not the unevolved potential (right shaded region).

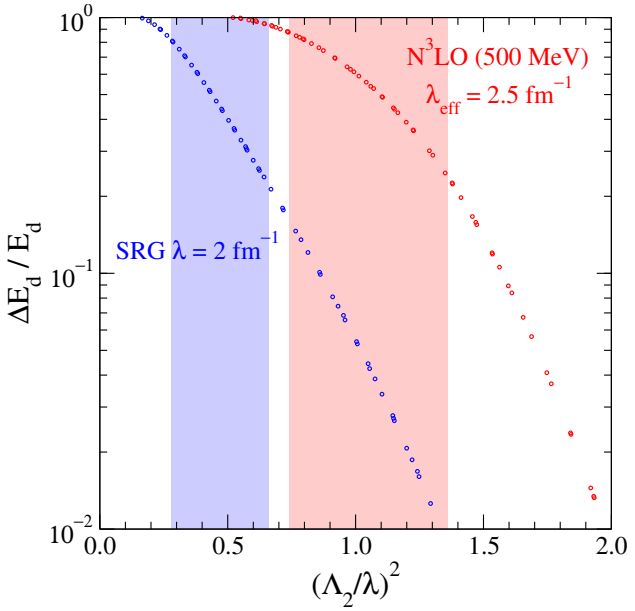

FIG. 21. (Color online) Relative error for the deuteron energy from HO basis truncation as a function of $(\Lambda_2/\lambda)^2$ for (N, Ω) values for which IR corrections can be neglected for the SRG-evolved N3LO potential by Entem and Machleidt (left) and the bare potential (right). Also indicated are the regions where the fit to a Gaussian was attempted.

V. FURTHER REMARKS

Before we summarize our results and conclude in the next section, we return here to some general remarks about the separable-approximation approach introduced in Sec. III.

A. More general derivation

While it was instructive to derive our general extrapolation formulas based on writing down a separable approximation for the original potential and then taking over the results obtained for explicitly separable interactions from Sec. III A, we can actually also take a more direct approach. If we consider a Hamiltonian $H = H_0 + V$ giving rise to a bound state $|\psi\rangle$ with binding energy $-E_B = -\kappa_\infty^2$, we can write the Schrödinger equation as

$$|\psi\rangle = G_0(-\kappa_\infty^2) V |\psi\rangle \,, \tag{76}$$

where G_0 is the Green's function (free resolvent)

$$G_0(z) = (z - H_0)^{-1} \,. \tag{77}$$

Acting with V on both sides and taking the matrix element with $\langle\psi|$, we get

$$1 = \frac{\langle\psi|V G_0(-\kappa_\infty^2) V|\psi\rangle}{\langle\psi|V|\psi\rangle} \,. \tag{78}$$

This already looks similar to our unitary-pole-approximation potential (32). Indeed, if we define $g \equiv \langle\psi|V|\psi\rangle^{-1}$ and $|\eta\rangle \equiv V|\psi\rangle$, we get

$$1 = g \times \langle\eta|G_0(-\kappa_\infty^2)|\eta\rangle \,, \tag{79}$$

or, explicitly in momentum space,

$$-1 = 4\pi g \int \mathrm{d}k \, \frac{k^2 \, \eta(k)^2}{\kappa_\infty^2 + k^2} \,. \tag{80}$$

Our extrapolation formulas follow from this if we assume that cutting off the integral at a cutoff Λ can be compensated by shifting $\kappa_\infty^2 \to \kappa_\Lambda^2 = \kappa_\infty^2 - \Delta E_\Lambda$.

Equation (79) is furthermore interesting because it might be possible to use it for deriving extrapolation relations for bound states of more than two particles by considering appropriate many-body Green's functions. Note also that as an alternative to Eq. (78) we can obtain from Eq. (76) a quantization condition of the form

$$1 = \frac{\langle\psi|G_0(-\kappa_\infty^2) V|\psi\rangle}{\langle\psi|\psi\rangle} \,. \tag{81}$$

This could be used to derive alternative extrapolation relations that involve $\psi(k)\eta(k)$ instead of $\eta(k)^2$. From the discussion in the following subsection, however, it will become clear that Eq. (80) is the better choice.

B. The form factors

If we look at the definition of the form factors $\eta(k)$ and assume that the state $|\psi\rangle$ is an exact solution of the Schrödinger equation (without truncation artifacts), it is clear that we can rewrite

$$\begin{aligned} \eta(k) = \langle k|V|\psi\rangle &= \langle k|G_0(-\kappa_\infty^2)^{-1}|\psi\rangle \\ &= (-\kappa_\infty^2 - k^2)\psi(k) \,. \end{aligned} \tag{82}$$

Using this, our extrapolation formulas can be rewritten in terms of $\psi(k)$ instead of $\eta(k)$, thus eliminating the explicit dependence on the potential. In our numerical calculations, however, we only have approximate solutions to the Schrödinger equation. While in principle one can carry out the above manipulations before making the *approximation* of using the numerically-determined wavefunctions, it turns out that in practice it works much better to use the extrapolations based on $\eta(k)$ unless the calculation is pretty much converged already.

The reason for this is likely that while the momentum-space wavefunction that comes out of a non-UV-converged oscillator calculation exhibits some unphysical structure due to truncation artifacts, the form factors calculated from it are still very smooth; integrating ψ with the potential V essentially removes the truncation artifacts. The effect is shown in Figs. 22 and 23 where we plot wavefunctions $u(k)$ and the corresponding separable form factors $\eta(k)$ as functions of k. The results were obtained using a Pöschl–Teller potential with $\alpha = 2/3$ and $\beta = 3$ in truncated oscillator bases with $b = 4.0$ fm. Clearly, even if the wavefunction is far from being converged, the corresponding $\eta(k)$ is smooth and close in shape to the known exact function (dashed curve). Note also that the UV cutoffs $\Lambda_2 \approx 1.2$ fm^{-1} ($n = 4$, Fig. 22) and $\Lambda_2 \approx 1.6$ fm^{-1} ($n = 8$, Fig. 23) are clearly visible in the oscillator-based wavefunction. Beyond the cutoff, they are essentially 0, which means that they are not suitable for extrapolations to larger cutoffs. This is different for the form factors, which still have high-momentum tails.

Finally, this analysis also shows that an extrapolation formula based on Eq. (81), featuring the product $u(k)\eta(k)$ would not work well with wavefunctions obtained from the truncated oscillator calculation.

VI. SUMMARY AND OUTLOOK

In this paper, we have developed a theoretical basis for UV errors in truncated harmonic oscillator spaces. We used the two-particle system with model potentials and deuteron calculations with realistic potentials as solvable theoretical laboratories to develop and test extrapolation schemes. By studying the two-body system in great detail, we follow the successful strategy of Refs. [7] and [8], which has recently led to successful extensions to the

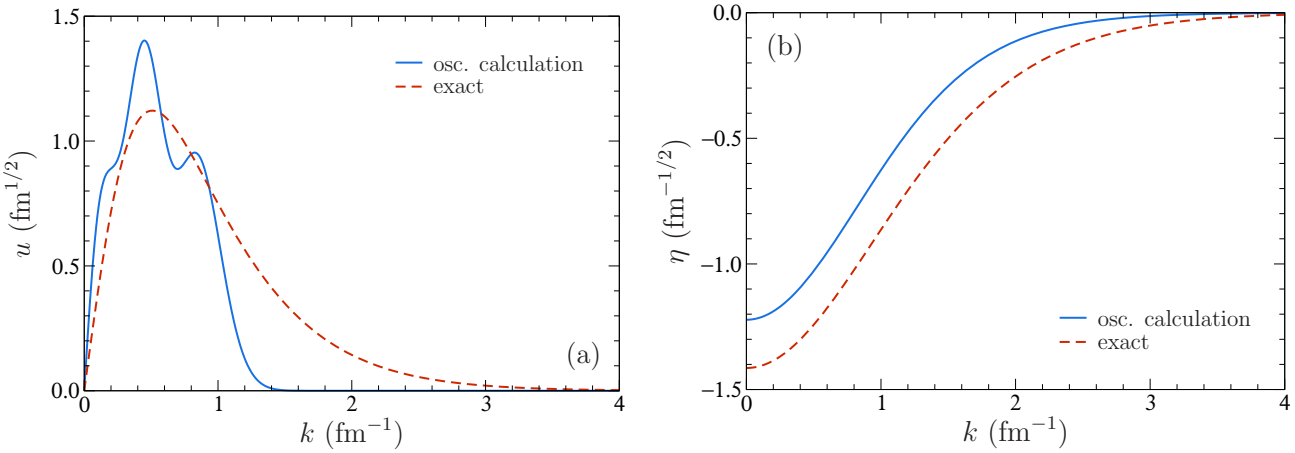

FIG. 22. (Color online) (a) Wave functions and (b) corresponding separable form factor for a Pöschl–Teller potential with $\alpha = 2/3$ and $\beta = 3$. Solid lines: results from oscillator calculation with $b = 4.0$ fm and $n = 4$. Dashed lines: exact (analytically known) results for comparison.

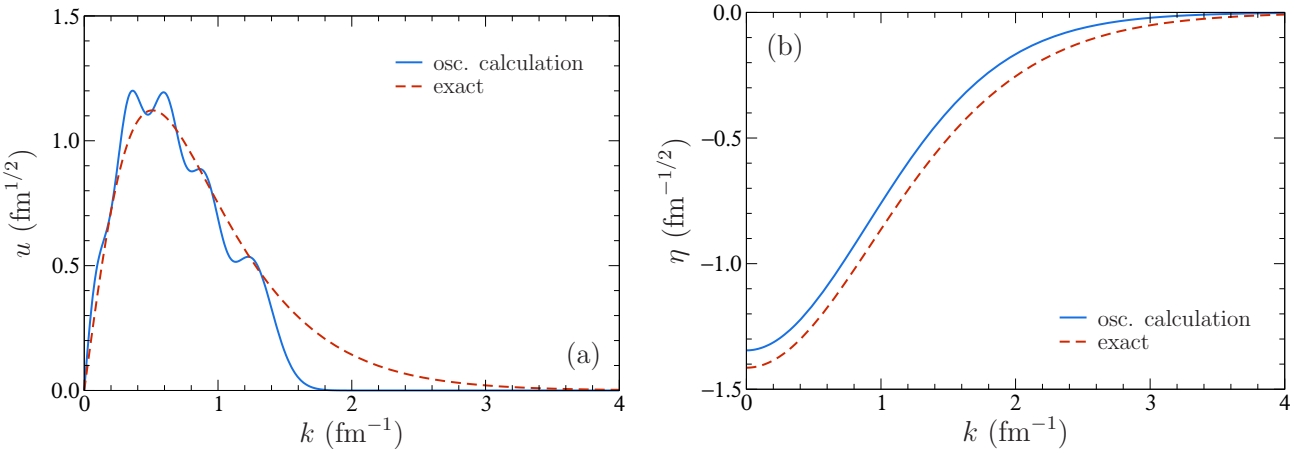

FIG. 23. (Color online) (a) Wave functions and (b) corresponding separable form factor for a Pöschl–Teller potential with $\alpha = 2/3$ and $\beta = 3$. Solid lines: results from oscillator calculation with $b = 4.0$ fm and $n = 8$. Dashed lines: exact (analytically known) results for comparison.

many-body sector [9]. First we established that the spectrum of the squared position operator in a finite oscillator basis is the same as that of a system with a hard cutoff in momentum. This is the dual result to the IR, where the spectrum of the squared momentum operator in a truncated oscillator basis coincides with that of a spherical box with a hard wall at radius L_2. Matching the lowest eigenvalues establishes the cutoff Λ_2, which was determined in a $1/N$ expansion. By duality, it is the same as L_2 (and beyond in $1/N$) when expressed in dimensionless units. The appropriateness of Λ_2 was verified by model and deuteron calculations, which showed a smooth curve with little scatter compared to other choices.

Having transferred the problem from calculations in a truncated basis to calculations with an imposed sharp momentum cutoff, we turned to rank-one separable potentials. For these potentials, we could directly derive an analytic formula for the correction to a bound-state eigenvalue in terms of integrals over the potential that relied on the correction being small. This formula was shown to be amenable to perturbation theory and asymptotic expansions when Λ_2 is greater than the intrinsic UV scale of the potential. This is useful for general tests and to establish that the UV correction depends on the high-momentum behavior of the potential.

But the true region of interest is when Λ_2 is comparable to or smaller than this scale. In this case, the integral expressions can be used to parametrize extrapolation formulas to fit. A new procedure was developed to generalize this extrapolation method to any potential by adapting the unitary pole approximation. Tests for model potentials as well as for the deuteron with realistic potentials are very encouraging. Finally, we showed how the simple Gaussian phenomenological extrapolation widely used in the past can be recovered from an expansion of the separable potential.

The IR and UV corrections exhibit a complementary mix of universal and non-universal characteristics. The IR corrections are dictated by asymptotic behavior and are consequently determined by observables, independent of the details of the interaction. So unitarily equivalent potentials—such as those generated by renormalization-group running—will have the same corrections. In contrast, because they probe short-range features, UV corrections depend on the details of the interaction (and the state under consideration). This was manifested here by the different corrections for the deuteron from SRG interactions at different resolutions as well as the explicit formulas with dependence on the high momentum behavior of the interaction.

On the other hand, the IR corrections are non-universal with respect to the number of nucleons A, depending for example on the separation energy of the nucleus. The dependence on A for the UV corrections is not yet established theoretically, but fits of the Gaussian ansatz Eq. (72) to energies from the same SRG-evolved potential for different values of A have been found to have roughly the same value of b_1 (approximately equal to $4/\lambda^2$, where λ is the SRG flow parameter [5, 11]). Thus the Λ_2 dependence is the same with ΔE_Λ just scaled by an A-dependent overall constant. For $A = 2$, ΔE_Λ is determined by the short-distance or high-momentum behavior. For $A > 2$, the many-body wave function is expected to factorize into a two-body part and a remainder when those two particle coordinates are sufficiently close. This can be understood from general considerations of short-range correlations [22] or more systematically using the operator product expansion [20, 23]. If there is a common two-body part, it may determine the dominant Λ_2 dependence (using the separable-approximation approach or at the level of the Gaussian approximation) with the rest providing the A-dependent scale factor. This behavior would be consistent with the observation of a universal shape for high-momentum tails in momentum distributions (or the corresponding short-distance behavior) [24]. This potential UV universality, as well as more direct approaches building on the discussion in Sec. V, is the subject of ongoing investigations.

ACKNOWLEDGMENTS

We thank M. Caprio, S. Coon, H.-W. Hammer, M. Kruse, R. Perry, R. Roth, and K. Wendt for useful discussions. Ideas that led to this publication were exchanged at the conference "Nuclear Theory in the Supercomputing Era (NTSE 2013)" in Ames, Iowa. This research was supported in part by the National Science Foundation under Grants No. PHY-1068648 (Michigan State University) and No. PHY–1306250 (Ohio State University), and by the U.S. Department of Energy, Office of Science, Office of Nuclear Physics, under Award Numbers DE-FG02-96ER40963 (University of Tennessee), and No. DE-SC0008499/DE-SC0008511/DE-SC0008533 (SciDAC-3 NUCLEI Collaboration) and under Contract No. DE-AC05-00OR22725 (Oak Ridge National Laboratory).

Appendix A: UV cutoff details

In this Appendix, we give a detailed derivation of the effective UV cutoff Λ_{eff} as a function of the HO parameters (basis size N and frequency Ω) that we report in Sec. II.

1. Notation and conventions

Consider the three-dimensional isotropic harmonic oscillator described by the Hamiltonian (in natural units with $\hbar = c = 1$)

$$H_{\text{HO}} = \frac{p^2}{2\mu} + \frac{\mu\Omega^2 r^2}{2}\,, \tag{A1}$$

where μ is the reduced mass and Ω denotes the oscillator frequency. The eigenstates $|n\ell m\rangle$ of H_{HO} are degenerate in the quantum number m,

$$H_{\text{HO}}|n\ell m\rangle = E_{n\ell m}|n\ell m\rangle \tag{A2}$$

with

$$E_{n\ell m} = \left(2n + \ell + \frac{3}{2}\right)\Omega\,. \tag{A3}$$

We use a slightly modified version of the conventions and notation from Ref. [25]. The full three-dimensional wavefunction in configuration space is

$$\psi_{n\ell m}(\mathbf{r}) = \langle \mathbf{r}|n\ell m\rangle = \frac{u_{n\ell}(b;r)}{r} Y_{\ell m}(\hat{\mathbf{r}}) \tag{A4}$$

with the reduced radial wavefunction

$$u_{n\ell}(b;r) = N_{n\ell}(b) \times (r/b)^{\ell+1} \mathrm{e}^{-(r/b)^2/2} L_n^{\ell+1/2}\big((r/b)^2\big)\,, \tag{A5}$$

where

$$N_{n\ell}(b) = \sqrt{\frac{2n!}{b\,\Gamma(n+\ell+3/2)}}\,, \tag{A6}$$

and

$$b = (\mu\Omega)^{-1/2} \tag{A7}$$

is the oscillator length. The Fourier transform of Eq. (A4) is

$$\tilde{\psi}_{n\ell m}(\mathbf{k}) = (2\pi)^{-3/2} \int \mathrm{d}^3 r\, \mathrm{e}^{-\mathrm{i}\mathbf{k}\cdot\mathbf{r}} \psi_{n\ell m}(\mathbf{r})\,. \tag{A8}$$

It can be written as

$$\tilde{\psi}_{n\ell m}(\mathbf{k}) = (-\mathrm{i})^\ell \frac{\widetilde{u}_{n\ell}(b;k)}{k} Y_{\ell m}(\hat{\mathbf{k}})\,, \tag{A9}$$

such that $\widetilde{u}_{n\ell}(b;k)$ is the Fourier–Bessel transform of $u_{n\ell}(b;r)$, *i.e.*,

$$\widetilde{u}_{n\ell}(b;k) = \sqrt{\frac{2}{\pi}} \int_0^\infty \mathrm{d}r'\, kr' j_\ell(kr')\, u_{n\ell}(b;r')\,. \tag{A10}$$

This gives

$$\widetilde{u}_{n\ell}(b;k) = (-1)^n \widetilde{N}_{n\ell}(b) \times (kb)^{\ell+1} \mathrm{e}^{-(kb)^2/2} L_n^{\ell+1/2}\big((kb)^2\big) \tag{A11}$$

with

$$\widetilde{N}_{n\ell}(b) = \sqrt{\frac{2n!\,b}{\Gamma(n+\ell+3/2)}}\,. \tag{A12}$$

2. Smallest eigenvalue of r^2

In the following derivation of Λ_{eff}, we directly consider subspaces with an arbitrary (but fixed) angular momentum ℓ, but quote S-wave ($\ell = 0$) results explicitly for the sake of illustration. Denoting the square root of the smallest eigenvalue of r^2 in the truncated oscillator subspace with angular momentum ℓ by ρ,[6] the localized momentum-space eigenfunction for a hard-wall (Dirichlet) boundary condition in momentum space is

$$\widetilde{\psi}_{\rho,\ell}(p) = \begin{cases} p\rho\, j_\ell(p\rho)\,, & 0 \le p \le x_\ell/\rho\,, \\ 0\,, & p > x_\ell/\rho\,, \end{cases} \tag{A13}$$

where x_ℓ denotes the smallest positive zero of the spherical Bessel function j_ℓ. For S-waves, one simply has $\widetilde{\psi}_{\rho,\ell}(p) = \sin(p\rho)$ and $x_0 = \pi$. The eigenfunction can be expanded in terms of oscillator functions as

$$\widetilde{\psi}_\rho(p) = \sum_{k=0}^\infty \widetilde{c}_k(\rho) \widetilde{u}_k(p)\,, \tag{A14}$$

without basis truncation so far. We have used the shorthand notation

$$\widetilde{u}_n(p) \equiv \widetilde{u}_{n\ell}(1;p)\,. \tag{A15}$$

In particular, we set the oscillator length b to unity for the time being. Exactly as in Ref. [7], the eigenvalue problem

$$\big[r^2 - \rho^2\big]\, \widetilde{\psi}_\rho(p) = 0 \tag{A16}$$

becomes a set of coupled linear equations. For S-waves, one can use the fact that the three-dimensional oscillator wavefunctions are directly related to the (odd) one-dimensional oscillator states and write

$$r^2 = a^\dagger a + \frac{1}{2} + \frac{1}{2}\left[a^2 + (a^\dagger)^2\right]\,, \tag{A17}$$

where a and $a^\dagger$ are ladder operators, to obtain (after shifting some indices)

$$\big[r^2 - \rho^2\big]\, \widetilde{\psi}_\rho(p) = 0 \iff \sum_{k=0}^\infty \Big[(2k+3/2-\rho^2)\widetilde{c}_k(\rho) - \frac{1}{2}\sqrt{2k+1}\sqrt{2k+3}\,\widetilde{c}_{k+1}(\rho) - \frac{1}{2}\sqrt{2k}\sqrt{2k+1}\,\widetilde{c}_{k-1}(\rho)\Big]\, \widetilde{u}_k(p) = 0 \quad (\ell = 0)\,. \tag{A18}$$

More generally, a direct evaluation yields (*cf.* the analogous results for p^2 given in Ref. [8])

$$\langle k\ell m|r^2|j\ell m\rangle = (2k+\ell+3/2)\delta_k^j + \sqrt{k+1}\sqrt{k+\ell+3/2}\,\delta_k^{j+1} + \sqrt{k}\sqrt{k+\ell+1/2}\,\delta_k^{j-1}\,, \tag{A19}$$

and thus we get

$$\big[r^2 - \rho^2\big]\, \widetilde{\psi}_\rho(p) = 0 \iff \sum_{k=0}^\infty \Big[(2k+\ell+3/2-\rho^2)\widetilde{c}_k(\rho) - \sqrt{k+1}\sqrt{k+\ell+3/2}\,\widetilde{c}_{k+1}(\rho) - \sqrt{k}\sqrt{k+\ell+1/2}\,\widetilde{c}_{k-1}(\rho)\Big]\, \widetilde{u}_k(p) = 0 \tag{A20}$$

for arbitrary angular momentum ℓ.

[6] Strictly, we should write ρ_ℓ here, but we omit the additional subscript for notational simplicity.

If the basis—and thus the sum in Eq. (A20)—is now truncated at some maximum $k \equiv n$, the last equation of the coupled set reads

$$(2n+\ell+3/2-\rho^2)\,\widetilde{c}_n(\rho) - \sqrt{n}\sqrt{n+\ell+1/2}\,\widetilde{c}_{n-1}(\rho) = 0\,. \tag{A21}$$

Further following Ref. [8], we introduce the Fourier–Bessel transform of $\widetilde{\psi}_\rho(p)$ as

$$\widetilde{\psi}_\rho(p) = \sqrt{\frac{2}{\pi}} \int_0^\infty \mathrm{d}r\, \psi_\rho(r)\, pr\, j_\ell(pr)\,, \tag{A22}$$

and use

$$pr\, j_\ell(pr) = \sqrt{\frac{\pi}{2}} \sum_{n=0}^{\infty} \widetilde{u}_{n\ell}(b;p) u_{n\ell}(b;r) \quad \text{for arbitrary } b \tag{A23}$$

to infer

$$\widetilde{c}_n(\rho) = \int_0^\infty \mathrm{d}r\, \psi_\rho(r) u_n(r) \tag{A24}$$

from Eq. (A14). To proceed, we use the asymptotic approximation [8, 26]

$$u_{n\ell}(b;r) \approx \frac{2^{1-n}}{\pi^{1/4}} \sqrt{\frac{(2n+2\ell+1)!}{b\,(n+\ell)!n!}} (4n-2\ell+3)^{-\frac{\ell+1}{2}} \times \sqrt{4n+2\ell+3}\,(r/b)\, j_\ell\left(\sqrt{4n+2\ell+3}\,(r/b)\right)\,, \tag{A25}$$

valid for $n \gg 1$. Defining

$$\beta_\ell = \sqrt{4n+2\ell+3} \tag{A26}$$

and still setting $b = 1$ at this point, we get

$$\begin{aligned} \widetilde{c}_n(\rho) &\approx \frac{2^{1-n}}{\pi^{1/4}} \sqrt{\frac{(2n+2\ell+1)!}{(n+\ell)!n!}} \\ &\quad \times \beta_\ell^{-\ell-1} \int_0^\infty \mathrm{d}r\, \psi_\rho(r)\, \beta_\ell r\, j_\ell(\beta_\ell r) \\ &= \frac{2^{1-n}}{\pi^{1/4}} \sqrt{\frac{(2n+2\ell+1)!}{(n+\ell)!n!}} \times \beta_\ell^{-\ell-1} \sqrt{\frac{\pi}{2}}\, \widetilde{\psi}_\rho(\beta_\ell) \\ &= \frac{\pi^{1/4}}{2^{n-1/2}} \sqrt{\frac{(2n+2\ell+1)!}{n!(n+\ell)!}} \times \beta_\ell^{-\ell} \rho\, j_\ell(\beta_\ell \rho)\,. \end{aligned} \tag{A27}$$

The intermediate and final steps here follow from Eqs. (A22) and (A13), respectively, and we have the constraint $\rho < x_\ell/\beta_\ell$. Inserting Eq. (A27) into the quantization condition (A21) gives an equation that is formally exactly the same as given in Ref. [8] for the IR case.[7]

[7] Some relative minus signs—compare, for example, Eq. (A21) to Eq. (31) in Ref. [8]—have dropped out along the way. Note also that Ref. [8] uses a slightly different convention for the momentum-space oscillator wavefunctions that does not involve the phase $(-1)^n$ in our Eq. (A11).

3. Cutoff identification

If we make the ansatz

$$\rho = \frac{x_\ell}{\sqrt{4n+2\ell+3+2\Delta}}\,, \tag{A28}$$

we get $\Delta = 2$ in the limit $n \gg 1$ and $n \gg \ell$, independent of ℓ. As we discuss in Appendix A 4, it is possible to derive subleading corrections to this result, which then depend on the angular momentum ℓ, but turn out to be numerically insignificant for all present practical applications.

With $N = 2n + \ell$, and restoring the oscillator length b by dimensional analysis, our result can also be written as

$$\rho = \frac{x_\ell b}{\sqrt{2}} \left(N + \frac{3}{2} + 2\right)^{-1/2}\,. \tag{A29}$$

This implies that the UV cutoff Λ_{eff} corresponding to the basis truncation at N is not given by the naive estimate

$$\Lambda_0 = \sqrt{2(N+3/2)}/b\,, \tag{A30}$$

which follows from $k = \sqrt{2\mu E}$ and Eq. (A3), but rather by

$$\Lambda_2 = \frac{x_\ell}{\rho} = \sqrt{2(N+3/2+2)}/b\,, \tag{A31}$$

completely dual to the configuration-space box size L_2 given in Eq. (1).

4. Subleading corrections to L_2 and Λ_2

It is possible to derive subleading corrections to the result $\Delta = 2$ that was derived in the previous subsection. Because of the duality of configuration-space and momentum-space oscillator wavefunctions, the results derived in the following apply directly also to the effective box size L_2 used to calculate IR corrections.

For the smallest eigenvalue ρ^2 of the operator r^2 in the (truncated) oscillator basis we now wish to make the general ansatz

$$\rho = \frac{x_\ell}{\sqrt{4n+2\ell+3+2\left(\Delta_0 + \dfrac{\Delta_1}{n} + \dfrac{\Delta_2}{n^2} + \cdots\right)}}\,. \tag{A32}$$

In principle, there is an infinite sum of terms with increasing inverse powers of n in Eq. (A32), but we only give explicit results here up to $\mathcal{O}(1/n^2)$.

In Sec. II A, the result $\Delta = \Delta_0 = 2$ was found by inserting (A27) into the quantization condition (A21) and then considering the limits $n \gg 1$ and $n \gg \ell$. In practice, this is done by inserting the ansatz for $\rho = \rho(n)$ into $\tilde{c}_n(\rho) \sim \rho\, j_\ell(\beta_\ell \rho)$ and keeping only the leading term in an asymptotic expansion around $n = \infty$.

To obtain the desired subleading corrections, it is however not sufficient to simply keep higher-order terms in this asymptotic expansion. Instead, one first has to go back a few steps and also keep higher-order corrections to the leading asymptotic approximation for the oscillator wavefunctions given in Eq. (A25). Note that this approximation follows from using Eq. (15) of Ref. [26], which states that the generalized Laguerre polynomials have the asymptotic expansion

$$L_n^\alpha(z) = \frac{\Gamma(n+\alpha+1)}{n!} \mathrm{e}^{z/2} \sum_{m=0}^{\infty} \left(\frac{z}{2}\right)^m P_m(\alpha+1,z) \times (\kappa z)^{-\frac{m+\alpha}{2}} J_{m+\alpha}(2\sqrt{\kappa z}) \quad \text{(A33)}$$

with

$$\kappa = n + \frac{\alpha+1}{2} \quad \text{(A34a)}$$

$$= n + \frac{3}{4} \quad \text{for} \quad \alpha = 1/2 \quad \text{(A34b)}$$

and

$$P_0(c,z) = 1 \quad , \quad P_1(c,z) = z/6 \quad , \quad \cdots . \quad \text{(A35)}$$

Using this in Eq. (A5) and keeping only the first ($m = 0$) term gives Eq. (A25). More generally, one finds that for large n the oscillator wavefunctions $u_{n\ell}(r)$ can be expressed as a sum

$$u_{n\ell}(r) = u_{n\ell}^{(0)}(r) + u_{n\ell}^{(1)}(r) + \cdots , \quad \text{(A36)}$$

where the individual terms involve (spherical) Bessel functions of increasing order. Recalling Eq. (A24), it then follows that also

$$\tilde{c}_n(\rho) = \tilde{c}_n^{(0)}(\rho) + \tilde{c}_n^{(1)}(\rho) + \cdots . \quad \text{(A37)}$$

We already know that

$$\tilde{c}_n^{(0)}(\rho) = C(n)\, \beta_\ell^{-\ell} \times \rho\, j_\ell(\beta_\ell \rho) \quad \text{(A38)}$$

with

$$C_\ell(n) = \frac{\pi^{1/4}}{2^{n-1/2}} \sqrt{\frac{(2n+2\ell+1)!}{n!(n+\ell)!}} . \quad \text{(A39)}$$

The key step in deriving Eq. (A38) was to express $\tilde{c}_n^{(0)}(\rho)$ in terms of $\tilde{\psi}_\rho$ by using the Fourier–Bessel transform, which could be done since asymptotically $u_{n\ell}^{(0)}(r)$ is simply proportional to $j_\ell(\beta_\ell \rho)$. More generally, for the individual terms in the expansion (A36) we have

$$u_{n\ell}^{(k)}(r) = \frac{2^{1-n}}{\pi^{1/4}} \sqrt{\frac{(2n+2\ell+1)!}{(n+\ell)!n!}} \beta_\ell^{-(\ell+k)} \times P_k(\ell+3/2, r^2) r^{k+1} j_{\ell+k}(\beta_\ell r) . \quad \text{(A40)}$$

This means that to obtain a generalization of Eq. (A27), we have to calculate expressions of the form

$$\tilde{c}_n^{(k)}(\rho) \sim \beta_\ell^{-(\ell+k)} \int_0^\infty \mathrm{d}r\, \psi_\rho(r)\, P_k(\ell+3/2, r^2) \times r^{k+1} j_{\ell+k}(\beta_\ell r) . \quad \text{(A41)}$$

To evaluate these integrals, it is more convenient to work with Riccati–Bessel functions,

$$\hat{\jmath}_\nu(z) = z j_\nu(z) , \quad \text{(A42)}$$

in terms of which we have

$$\tilde{c}_n^{(k)}(\rho) \sim \beta_\ell^{-(\ell+k+1)} \int_0^\infty \mathrm{d}r\, \psi_\rho(r)\, P_k(\ell+3/2, r^2) \times r^k \hat{\jmath}_{\ell+k}(\beta_\ell r) . \quad \text{(A43)}$$

For the Riccati–Bessel functions one has the derivative relation [27]

$$\frac{\partial \hat{\jmath}_\nu(z)}{\partial z} = \frac{\nu+1}{z} \hat{\jmath}_\nu(z) - \hat{\jmath}_{\nu+1}(z) , \quad \text{(A44)}$$

from which it follows straightforwardly that

$$\hat{\jmath}_{\nu+1}(\beta r) = \frac{1}{r} \left[\frac{\nu+1}{\beta} - \frac{\mathrm{d}}{\mathrm{d}\beta}\right] \hat{\jmath}_\nu(\beta r) . \quad \text{(A45)}$$

Using this relation k times in Eq. (A41), we can eliminate the prefactor r^k in favor of a differential operator with respect to a variable β,

$$\tilde{c}_n^{(k)}(\rho) \sim \beta_\ell^{-(\ell+k+1)} \int_0^\infty \mathrm{d}r\, \psi_\rho(r)\, P_k(\ell+3/2, r^2) \times \left(\frac{\ell+k}{\beta} - \frac{\mathrm{d}}{\mathrm{d}\beta}\right) \left(\frac{\ell+k-1}{\beta} - \frac{\mathrm{d}}{\mathrm{d}\beta}\right) \cdots \left(\frac{\ell}{\beta} - \frac{\mathrm{d}}{\mathrm{d}\beta}\right) \times \hat{\jmath}_\ell(\beta r)\Big|_{\beta=\beta_\ell} . \quad \text{(A46)}$$

At this point, we have also conveniently reduced the order of the Riccati–Bessel functions so that we have the same function for each $\tilde{c}_n^{(k)}(\rho)$; all remaining additional r-dependence comes from the $P_k(\ell+3/2, r^2)$, which are polynomials in r^2. This can also be eliminated by noting that

$$r^2 \hat{\jmath}_\ell(\beta r) = \left(-\frac{\mathrm{d}^2}{\mathrm{d}\beta^2} + \frac{\ell(\ell+1)}{\beta^2}\right) \hat{\jmath}_\ell(\beta r) , \quad \text{(A47)}$$

which follows immediately from the differential equations that defines the Riccati–Bessel functions and is formally just the free radial Schrödinger equation if one interchanges the variables r and β. Altogether, we have found that we can write

$$\tilde{c}_n^{(k)}(\rho) \sim \beta_\ell^{-(\ell+k+1)} \int_0^\infty \mathrm{d}r\, \psi_\rho(r)\, \mathcal{D}_{\beta,\ell}^{(k)} \hat{\jmath}_\ell(\beta r)\Big|_{\beta=\beta_\ell} , \quad \text{(A48)}$$

where $\mathcal{D}^{(k)}_{\beta,\ell}$ is some differential operator (with respect to β) which can be pulled out of the integral. The precise form of this operator can be obtained from the equations above, but it is actually not important here. At this point we can proceed exactly as in Eq. (A27) and write, restoring the full prefactor,

$$\begin{aligned}\tilde{c}^{(k)}_n(\rho) &= \frac{2^{1-n}}{\pi^{1/4}}\sqrt{\frac{(2n+2\ell+1)!}{(n+\ell)!n!}}\,\beta_\ell^{-(\ell+k+1)} \\ &\quad\times \mathcal{D}^{(k)}_{\beta,\ell}\int_0^\infty \mathrm{d}r\,\psi_\rho(r)\,\hat{\jmath}_\ell(\beta r)\,\Big|_{\beta=\beta_\ell} \\ &= \frac{2^{1-n}}{\pi^{1/4}}\sqrt{\frac{(2n+2\ell+1)!}{(n+\ell)!n!}}\,\beta_\ell^{-(\ell+k+1)} \\ &\quad\times \sqrt{\frac{\pi}{2}}\,\mathcal{D}^{(k)}_{\beta,\ell}\,\tilde{\psi}_\rho(\beta)\,\Big|_{\beta=\beta_\ell} \\ &= C_\ell(n)\,\beta_\ell^{-(\ell+k+1)}\times \mathcal{D}^{(k)}_{\beta,\ell}\,\hat{\jmath}(\beta\rho)\Big|_{\beta=\beta_\ell} \\ &= C_\ell(n)\,\beta_\ell^{-\ell-k}\times P_k(\ell+3/2,\rho^2)\,\rho^{k+1} j_{\ell+k}(\beta_\ell\rho)\,.\end{aligned}$$

We have used here that $\tilde{\psi}_\rho(\beta) = \beta\rho\, j_\ell(\beta\rho) = \hat{\jmath}(\beta\rho)$ for $\beta \le x_\ell/\rho$, and that we can ultimately apply the operator $\mathcal{D}^{(k)}_{\beta,\ell}$ to get back the original expression as in Eq. (A41), only with r replaced by ρ. The coefficients $C_\ell(n)$ have been defined in Eq. (A39).

With these general expressions for all terms in the expansion of $\tilde{c}_n(\rho)$, we can now write the quantization condition (A21) as

$$\begin{aligned}&(2n+\ell+3/2-\rho^2)\times\sum_{k=0}^{k_\mathrm{max}}\tilde{c}^{(k)}_n(\rho) \\ &\qquad -\sqrt{n}\sqrt{n+\ell+1/2}\times\sum_{k=0}^{k_\mathrm{max}}\tilde{c}^{(k)}_{n-1}(\rho) = 0\,. \quad \text{(A49)}\end{aligned}$$

The appropriate truncation index k_max in this equation depends on both ℓ and the desired order for the subleading corrections. To solve for these, we insert an ansatz of the form (A32) into Eq. (A49) and solve for the coefficients Δ_0, Δ_1, etc. by performing an asymptotic expansion around $n=\infty$. To do this consistently, it is important to keep all terms that can contribute to the maximum order we are interested in. In general, there are cancellations between the polynomial prefactors $P_k(\ell+3/2,\rho^2)\times\rho^{k+1}$ and the spherical Bessel functions $j_{\ell+k}(\beta_\ell\rho)$ since the latter contribute inverse powers of $\beta_\ell\rho$, which become more prominent with increasing ℓ. At least for $\ell=0$ and $\ell=1$ we find that $k_\mathrm{max}=2$ is sufficient to get the corrections up to and including $\mathcal{O}(1/n^2)$. The results, obtained with computer algebra software (Wolfram Mathematica), are

$$\ell=0:\quad \Delta_1 = \frac{3-2\pi^2}{48}\,,\qquad \Delta_2 = \frac{-7(3-2\pi^2)}{192}\,, \quad \text{(A50)}$$

$$\ell=1:\quad \Delta_1 = \frac{1}{48}(3-2\pi^2)\,,\quad \Delta_2 = \frac{3(5+2x_1^2)}{64}\,. \quad \text{(A51)}$$

One always has $\Delta_0 = 2$, independent of ℓ.

TABLE III. Comparison of the smallest distance scale ρ at different orders in the $1/n$ expansion to the exact answer for several values of n. S-wave results ($\ell=0$).

n	ρ, $\mathcal{O}(1/n^0)$	ρ, $\mathcal{O}(1/n^1)$	ρ, $\mathcal{O}(1/n^2)$	ρ, exact
1	0.94723	0.97876	0.92548	0.95857
2	0.81116	0.82075	0.81234	0.81629
3	0.72073	0.72518	0.72258	0.72355
4	0.65507	0.65756	0.65647	0.65681
5	0.60460	0.60617	0.60562	0.60576
6	0.56425	0.56531	0.56500	0.56507
7	0.53103	0.53178	0.53159	0.53163
8	0.50306	0.50362	0.50350	0.50352
9	0.47909	0.47952	0.47944	0.47945
10	0.45825	0.45859	0.45853	0.45854
11	0.43991	0.44018	0.44014	0.44015
12	0.42361	0.42384	0.42380	0.42381

TABLE IV. Comparison of the smallest distance scale ρ at different orders in the $1/n$ expansion to the exact answer for several values of n. P-wave results ($\ell=1$).

n	ρ, $\mathcal{O}(1/n^0)$	ρ, $\mathcal{O}(1/n^1)$	ρ, $\mathcal{O}(1/n^2)$	ρ, exact
1	1.2462	1.3481	1.1464	1.2764
2	1.0898	1.1214	1.0860	1.1047
3	0.98054	0.99560	0.98424	0.98920
4	0.89868	0.90730	0.90242	0.90423
5	0.83441	0.83990	0.83741	0.83821
6	0.78220	0.78596	0.78455	0.78495
7	0.73871	0.74142	0.74055	0.74077
8	0.70175	0.70378	0.70321	0.70334
9	0.66984	0.67141	0.67101	0.67110
10	0.64192	0.64316	0.64288	0.64293
11	0.61722	0.61822	0.61802	0.61805
12	0.59517	0.59599	0.59584	0.59586

In Tables III and IV we show (for $\ell=0$ and $\ell=1$, respectively) how subsequent inclusion of the correction terms makes the values for ρ as defined in Eq. (A32) converge to the exact results, which have been calculated numerically.

Appendix B: Pöschl–Teller states and form factors

In this Appendix we provide some details about the wavefunctions and separable form factors $\eta(k)$ for the Pöschl–Teller potential used in Sec. III B. In the conventions of Flügge's textbook [28], this potential can be written as[8]

$$V_{\rm PT}(r) = -\frac{\alpha^2\beta(\beta-1)}{\cosh^2(\alpha r)} \tag{B1}$$

Labeling different states with an index ν, we can write their wavefunctions as

$$\psi_{\beta\nu}(\alpha;r) = \frac{\sqrt{2}}{r}\cosh^\beta(\alpha r)\sinh(\alpha r) \times {}_2F_1\Big(\nu+\frac{3}{2},\beta-\nu-\frac{1}{2},\frac{3}{2};-\sinh^2(\alpha r)\Big)\,, \tag{B2}$$

where ${}_2F_1$ is the hypergeometric function [14]. The first odd bound state with nonzero energy occurs for $\beta = 3, \nu = 0$, and has a binding momentum $\kappa = \alpha$. For $\beta = 4$, there are two odd bound states, one of which has zero energy. For $\beta = 5$ one finds two odd bound states at $\kappa = 3\alpha$ ($\nu = 0$) and $\kappa = \alpha$ ($\nu = 1$). With Eq. (B2) it is straightforward to obtain the separable approximations for these states. We find

$$\eta_{\rm PT}(k) = -\frac{\sqrt{2}\,(k^2+\alpha^2)}{\alpha^2\cosh\big(\frac{\pi k}{2\alpha}\big)}\quad,$$
$$g_{\rm PT} = -\frac{5\pi}{16\alpha}\quad\text{for}\quad\beta=3\quad\text{and}\quad\nu=0\,, \tag{B3}$$

and

$$\eta_{\rm PT}(k) = -\frac{\sqrt{2}\,(k^2+\alpha^2)(k^2+9\alpha^2)}{6\alpha^4\cosh\big(\frac{\pi k}{2\alpha}\big)}\quad,\quad g_{\rm PT} = -\frac{63\pi}{256\alpha}$$
$$\text{for}\quad\beta=5\quad\text{and}\quad\nu=0\,, \tag{B4a}$$
$$\eta_{\rm PT}(k) = -\frac{\sqrt{2}\,(k^2+\alpha^2)(-7k^2+17\alpha^2)}{18\alpha^4\cosh\big(\frac{\pi k}{2\alpha}\big)}\quad,\quad g_{\rm PT} = -\frac{81\pi}{256\alpha}$$
$$\text{for}\quad\beta=5\quad\text{and}\quad\nu=1\,. \tag{B4b}$$

It is straightforward to obtain results also for higher values of β, but we restrict ourselves to these representative examples here.

[1] I. Stetcu, B. R. Barrett, and U. van Kolck, Phys. Lett. B **653**, 358 (2007).
[2] G. Hagen, T. Papenbrock, D. J. Dean, and M. Hjorth-Jensen, Phys. Rev. C **82**, 034330 (2010).
[3] E. D. Jurgenson, P. Navratil, and R. J. Furnstahl, Phys. Rev. C **83**, 034301 (2011).
[4] S. A. Coon, M. I. Avetian, M. K. Kruse, U. van Kolck, P. Maris, and J. P. Vary, Phys. Rev. C **86**, 054002 (2012).
[5] R. J. Furnstahl, G. Hagen, and T. Papenbrock, Phys. Rev. C **86**, 031301 (2012).
[6] S. A. Coon and M. K. G. Kruse, (2014).
[7] S. N. More, A. Ekström, R. J. Furnstahl, G. Hagen, and T. Papenbrock, Phys. Rev. C **87**, 044326 (2013).
[8] R. J. Furnstahl, S. N. More, and T. Papenbrock, Phys. Rev. C **89**, 044301 (2014).
[9] R. J. Furnstahl, G. Hagen, T. Papenbrock, and K. A. Wendt, (2014).
[10] D. Ernst, C. Shakin, and R. Thaler, Phys. Rev. C **8**, 46 (1973).
[11] E. D. Jurgenson, P. Maris, R. J. Furnstahl, P. Navrátil, W. E. Ormand, and J. P. Vary, Phys. Rev. C **87**, 054312 (2013).
[12] D. R. Entem and R. Machleidt, Phys. Rev. C **68**, 041001 (2003).
[13] S. K. Bogner, R. J. Furnstahl, and R. J. Perry, Phys. Rev. C **75**, 061001 (2007).
[14] F. W. J. Olver, D. W. Lozier, R. F. Boisvert, and C. W. Clark, eds., *NIST Handbook of Mathematical Functions* (Cambridge University Press, New York, NY, 2010).
[15] E. Harms, Phys. Rev. C **1**, 1667 (1970).
[16] O. Elgarøy and M. Hjorth-Jensen, Phys. Rev. C **57**, 1174 (1998).
[17] C. Lovelace, Phys. Rev. **135**, B1225 (1964).
[18] G. Bund and M. Tibero, Nuovo Cim. A **57**, 234 (1980).
[19] E. R. Anderson, S. K. Bogner, R. J. Furnstahl, and R. J. Perry, Phys. Rev. C **82**, 054001 (2010).
[20] S. K. Bogner and D. Roscher, Phys. Rev. C **86**, 064304 (2012).
[21] S. K. Bogner, R. J. Furnstahl, S. Ramanan, and A. Schwenk, Nucl. Phys. A **784**, 79 (2007).
[22] J. Kimball, Phys. Rev. A **7**, 1648 (1973).
[23] J. Hofmann, M. Barth, and W. Zwerger, Phys. Rev. B **87**, 235125 (2013).
[24] H. Feldmeier, W. Horiuchi, T. Neff, and Y. Suzuki, Phys. Rev. C **84**, 054003 (2011).
[25] M. A. Caprio, P. Maris, and J. P. Vary, Phys. Rev. C **86**, 034312 (2012).
[26] A. Deaño, E. J. Huertas, and F. Marcellán, J. Math. Anal. Appl. **403**, 477 (2013).
[27] M. Abramowitz and I. A. Stegun, *Handbook of Mathematical Functions* (Dover, New York, 1972).
[28] S. Flügge, ed., *Practical Quantum Mechanics* (Springer-Verlag, Berlin, 1999).

[8] Compared to Ref. [28] we have slightly changed the notation here by writing "β" instead of "λ" (to avoid confusion with the scale λ in Sec. III A), and "ν" instead of "m" (to label the states).